

STAR FORMATION IN GALAXIES ALONG THE HUBBLE SEQUENCE

Robert C. Kennicutt, Jr.

Steward Observatory, University of Arizona, Tucson, Arizona 85721;

e-mail: rkennicutt@as.arizona.edu

KEY WORDS: galaxy evolution, starbursts, spiral galaxies, star formation rates, stellar populations

ABSTRACT

Observations of star formation rates (SFRs) in galaxies provide vital clues to the physical nature of the Hubble sequence and are key probes of the evolutionary histories of galaxies. The focus of this review is on the broad patterns in the star formation properties of galaxies along the Hubble sequence and their implications for understanding galaxy evolution and the physical processes that drive the evolution. Star formation in the disks and nuclear regions of galaxies are reviewed separately, then discussed within a common interpretive framework. The diagnostic methods used to measure SFRs are also reviewed, and a self-consistent set of SFR calibrations is presented as an aid to workers in the field.

1. INTRODUCTION

One of the most recognizable features of galaxies along the Hubble sequence is the wide range in young stellar content and star formation activity. This variation in stellar content is part of the basis of the Hubble classification itself (Hubble 1926), and understanding its physical nature and origins is fundamental to understanding galaxy evolution in its broader context. This review deals with the global star formation properties of galaxies, the systematics of those properties along the Hubble sequence, and their implications for galactic evolution. I interpret “Hubble sequence” in this context very loosely, to encompass not only morphological type but other properties such as gas content, mass, bar structure, and dynamical environment, which can strongly influence the large-scale star formation rate (SFR).

Systematic investigations of the young stellar content of galaxies trace back to the early studies of resolved stellar populations by Hubble and Baade and analyses of galaxy colors and spectra by Stebbins, Whitford, Holmberg, Humason, Mayall, Sandage, Morgan, and de Vaucouleurs (see Whitford 1975 for a summary of the early work in this field). This piecemeal information was synthesized by Roberts (1963), in an article for the first volume of the *Annual Review of Astronomy and Astrophysics*. Despite the limited information that was available on the SFRs and gas contents of galaxies, Roberts' analysis established the basic elements of the contemporary picture of the Hubble sequence as a monotonic sequence in present-day SFRs and past star formation histories.

Quantifying this picture required the development of more precise diagnostics of global SFRs in galaxies. The first quantitative SFRs were derived from evolutionary synthesis models of galaxy colors (Tinsley 1968, 1972, Searle et al 1973). These studies confirmed the trends in SFRs and star formation histories along the Hubble sequence and led to the first predictions of the evolution of the SFR with cosmic lookback time. Subsequent modeling of blue galaxies by Bagnuolo (1976), Huchra (1977), and Larson & Tinsley (1978) revealed the importance of star formation bursts in the evolution of low-mass galaxies and interacting systems. Over the next decade, the field matured fully, with the development of more precise direct SFR diagnostics, including integrated emission-line fluxes (Cohen 1976, Kennicutt 1983a), near-ultraviolet continuum fluxes (Donas & Deharveng 1984), and infrared (IR) continuum fluxes (Harper & Low 1973, Rieke & Lebofsky 1978, Telesco & Harper 1980). These provided absolute SFRs for large samples of nearby galaxies, and these were subsequently interpreted in terms of the evolutionary properties of galaxies by Kennicutt (1983a), Gallagher et al (1984), and Sandage (1986).

Activity in this field has grown enormously in the past decade, stimulated in large part by two major revelations. The first was the discovery of a large population of ultraluminous IR starburst galaxies by the Infrared Astronomical Satellite (IRAS) in the mid-1980s. Starbursts had been identified (and coined) from groundbased studies (Rieke & Lebofsky 1979, Weedman et al 1981), but IRAS revealed the ubiquity of the phenomenon and the extreme nature of the most luminous objects. The latest surge of interest in the field has been stimulated by the detection of star-forming galaxies at high redshift, now exceeding $z = 3$ (Steidel et al 1996, Ellis 1997). This makes it possible to apply the locally calibrated SFR diagnostics to distant galaxies and to directly trace the evolution of the SFR density and the Hubble sequence with cosmological lookback time.

The focus of this review is on the broad patterns in the star formation properties of galaxies and their implications for the evolutionary properties of the Hubble sequence. It begins with a summary of the diagnostic methods used to measure SFRs in galaxies, followed by a summary of the systematics of SFRs

along the Hubble sequence and the interpretation of those trends in terms of galaxy evolution. It concludes with a brief discussion of the physical regulation of the SFR in galaxies and future prospects in this field. Galaxies exhibit a huge dynamic range in SFRs, over six orders of magnitude even when normalized per unit area and galaxy mass, and the continuity of physical properties over this entire spectrum of activities is a central theme of this review.

With this broad approach in mind, I cannot begin to review the hundreds of important papers on the star formation properties of individual galaxies or the rich theoretical literature on this subject. Fortunately, there are several previous reviews in this series that provide thorough discussions of key aspects of this field. A broad review of the physical properties of galaxies along the Hubble sequence can be found in Roberts & Haynes (1994). The star formation and evolutionary properties of irregular galaxies are reviewed by Gallagher & Hunter (1984). The properties of IR-luminous starbursts are the subject of several reviews, most recently those by Soifer et al (1987), Telesco (1988), and Sanders & Mirabel (1996). Finally, an excellent review of faint blue galaxies by Ellis (1997) describes many applications to high-redshift objects.

2. DIAGNOSTIC METHODS

Individual young stars are unresolved in all but the closest galaxies, even with the *Hubble Space Telescope* (HST), so most information on the star formation properties of galaxies comes from integrated light measurements in the ultraviolet (UV), far-infrared (FIR), or nebular recombination lines. These direct tracers of the young stellar population have largely supplanted earlier SFR measures based on synthesis modeling of broadband colors, though the latter are still applied to multicolor observations of faint galaxies. This section begins with a brief discussion of synthesis models, which form the basis of all of the methods, followed by more detailed discussions of the direct SFR tracers.

2.1 *Integrated Colors and Spectra, Synthesis Modeling*

The basic trends in galaxy spectra with Hubble type are illustrated in Figure 1, which shows examples of integrated spectra for E, Sa, Sc, and Magellanic irregular galaxies (Kennicutt 1992b). When progressing along this sequence, several changes in the spectrum are apparent: a broad rise in the blue continuum, a gradual change in the composite stellar absorption spectrum from K-giant dominated to A-star dominated, and a dramatic increase in the strengths of the nebular emission lines, especially $H\alpha$.

Although the integrated spectra contain contributions from the full range of stellar spectral types and luminosities, it is easy to show that the dominant contributors at visible wavelengths are intermediate-type main sequence stars

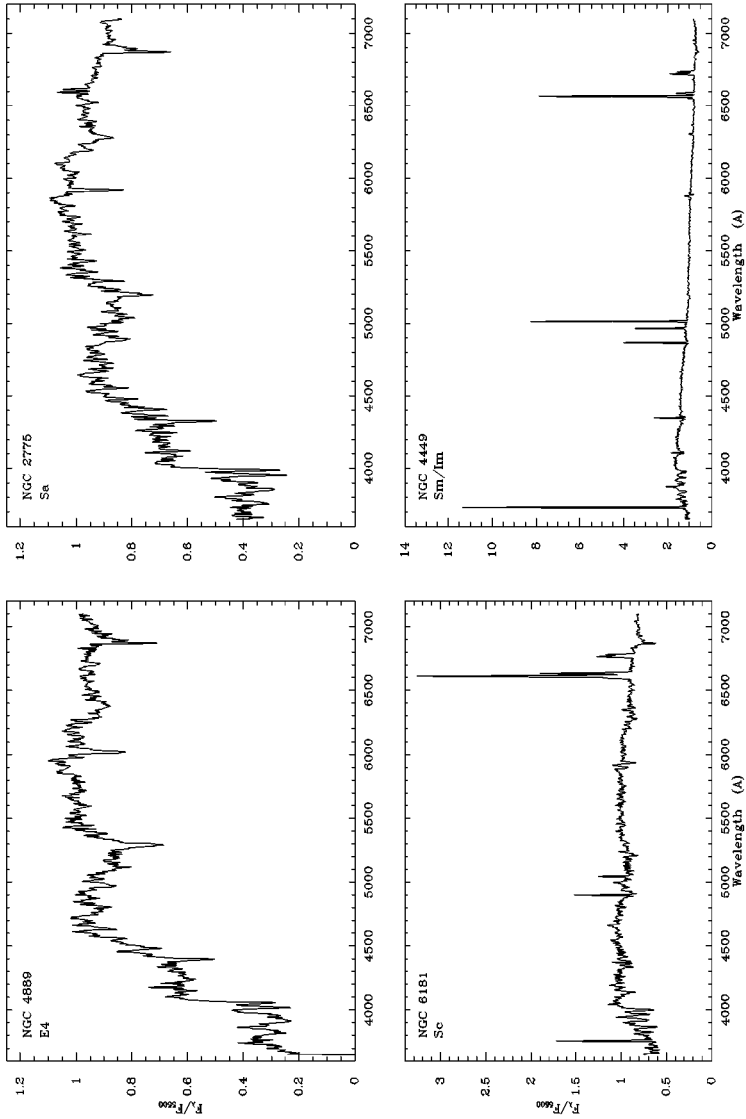


Figure 1 Integrated spectra of elliptical, spiral, and irregular galaxies, from Kennicutt (1992b). The fluxes have been normalized to unity at 5500 Å.

(A to early F) and G-K giants. As a result, the integrated colors and spectra of normal galaxies fall on a relatively tight sequence, with the spectrum of any given object dictated by the ratio of early- to late-type stars or, alternatively, by the ratio of young (<1 Gyr) to old (3–15 Gyr) stars. This makes it possible to use the observed colors to estimate the fraction of young stars and the mean SFR over the past 10^8 – 10^9 years.

The simplest application of this method would assume a linear scaling between the SFR and the continuum luminosity integrated over a fixed bandpass in the blue or near-ultraviolet. Although this may be a valid approximation in starburst galaxies, where young stars dominate the integrated light across the visible spectrum, the approximation breaks down in most normal galaxies, where a considerable fraction of the continuum is produced by old stars, even in the blue (Figure 1). However, the scaling of the SFR to continuum luminosity is a smooth function of the color of the population, and this can be calibrated using an evolutionary synthesis model.

Synthesis models are used in all of the methods described here, so it is useful to summarize the main steps in the construction of a model. A grid of stellar evolution tracks is used to derive the effective temperatures and bolometric luminosities for various stellar masses as a function of time, and these are converted into broadband luminosities (or spectra) using stellar atmosphere models or spectral libraries. The individual stellar templates are then summed together, weighted by an initial mass function (IMF), to synthesize the luminosities, colors, or spectra of single-age populations as functions of age. These isochrones can then be added in linear combination to synthesize the spectrum or colors of a galaxy with an arbitrary star formation history, usually parametrized as an exponential function of time. Although a single model contains at least four free parameters (the star formation history, galaxy age, metal abundance, and IMF), the colors of normal galaxies are well represented by a one-parameter sequence with fixed age, composition, and IMF, varying only in the time dependence of the SFR (Searle et al 1973, Larson & Tinsley 1978, Charlot & Bruzual 1991).

Synthesis models have been published by several authors and are often available in digital form. An extensive library of models has been compiled by Leitherer et al (1996a), and the models are described in a companion conference volume (Leitherer et al 1996b). Widely used models for star forming galaxies include those of Bruzual & Charlot (1993), Bertelli et al (1994), and Fioc & Rocca-Volmerange (1997). Leitherer & Heckman (1995) have published an extensive grid of models that is optimized for applications to starburst galaxies.

The synthesis models provide relations between the SFR per unit mass or luminosity and the integrated color of the population. An example is given in Figure 2, which plots the SFR per unit of U , B , and V luminosity as functions of $U - V$ color, based on the models of Kennicutt et al (1994). Figure 2 confirms that the broadband luminosity by itself is a poor tracer of the SFR; even the

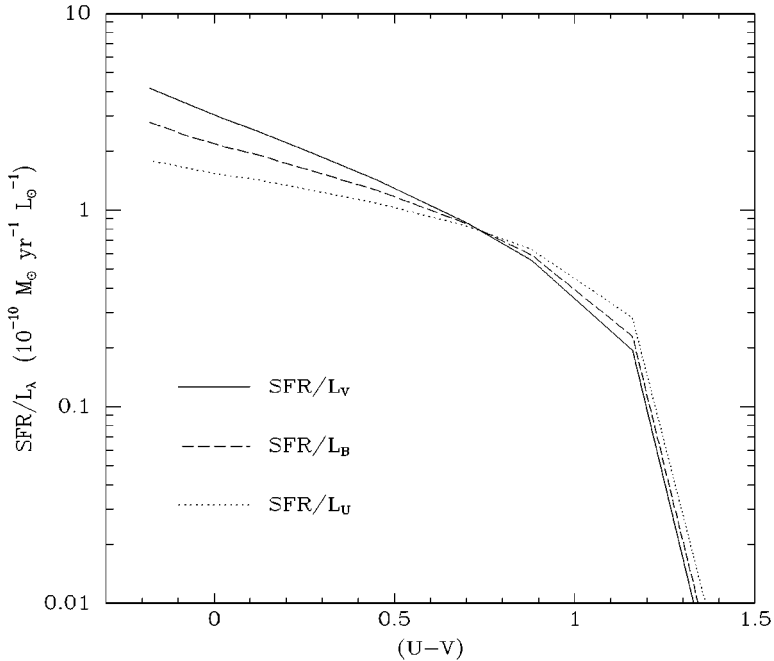


Figure 2 Relationship between star formation rate (SFR) per unit broadband luminosity in the *UBV* passbands and integrated color, from the evolutionary synthesis models of Kennicutt et al (1994). The models are for 10-billion-year-old disks, a Salpeter IMF, and exponential star formation histories. The *U*, *B*, and *V* luminosities are normalized to those of the Sun in the respective bandpasses.

SFR/L_U ratio varies by more than an order of magnitude over the relevant range of galaxy colors. However, the integrated color provides a reasonable estimate of the SFR per unit of luminosity, especially for the bluer galaxies.

The SFRs derived in this way are relatively imprecise and are prone to systematic errors from reddening or from an incorrect IMF, age, or metallicity of star formation history (Larson & Tinsley 1978). Nevertheless, the method offers a useful means of comparing the average SFR properties of large samples of galaxies when absolute accuracy is not required. The method should be avoided in applications where the dust content, abundances, or IMFs are likely to change systematically across a population.

2.2 *Ultraviolet Continuum*

The limitations described above can be avoided if observations are made at wavelengths where the integrated spectrum is dominated by young stars, so

that the SFR scales linearly with luminosity. The optimal wavelength range is 1250–2500 Å, longward of the Ly α forest but short enough to minimize spectral contamination from older stellar populations. These wavelengths are inaccessible from the ground for local galaxies ($z < 0.5$), but the region can be observed in the redshifted spectra of galaxies at $z \sim 1$ –5. The recent detection of the redshifted UV continua of large numbers of $z > 3$ galaxies with the Keck telescope has demonstrated the enormous potential of this technique (Steidel et al 1996).

The most complete UV studies of nearby galaxies are based on dedicated balloon, rocket, and space experiments (Smith & Cornett 1982, Donas & Deharveng 1984, Donas et al 1987, 1995, Buat 1992, Deharveng et al 1994). The database of high-resolution UV imaging of galaxies is improving rapidly, mainly from HST (Meurer et al 1995, Maoz et al 1996) and the *Ultraviolet Imaging Telescope* (Smith et al 1996, Fanelli et al 1997). An atlas of UV spectra of galaxies from the *International Ultraviolet Explorer* has been published by Kinney et al (1993). A recent conference volume by Waller et al (1997) highlights recent UV observations of galaxies.

The conversion between the UV flux over a given wavelength interval and the SFR can be derived using the synthesis models described earlier. Calibrations have been published by Buat et al (1989), Deharveng et al (1994), Leitherer et al (1995b), Meurer et al (1995), Cowie et al (1997), and Madau et al (1998) for wavelengths in the range 1500–2800 Å. The calibrations differ over a full range of ~ 0.3 dex, when converted to a common reference wavelength and IMF, with most of the difference reflecting the use of different stellar libraries or different assumptions about the star formation time scale. For integrated measurements of galaxies, it is usually appropriate to assume that the SFR has remained constant over time scales that are long compared with the lifetimes of the dominant UV emitting population ($< 10^8$ year), in the “continuous star formation” approximation. Converting the calibration of Madau et al (1998) to Salpeter’s (1955) IMF with mass limits 0.1 and 100 M_{\odot} yields

$$\text{SFR}(M_{\odot} \text{ year}^{-1}) = 1.4 \times 10^{-28} L_{\nu} (\text{ergs s}^{-1} \text{ Hz}^{-1}). \quad (1)$$

For a Salpeter IMF, the composite UV spectrum happens to be nearly flat in L_{ν} , over the wavelength range 1500–2800 Å, and this allows us to express the conversion in Equation 1 in such simple form. The corresponding conversion in terms of L_{λ} will scale as λ^{-2} . Equation 1 applies to galaxies with continuous star formation over time scales of 10^8 years or longer; the SFR/ L_{ν} ratio will be significantly lower in younger populations such as young starburst galaxies. For example, continuous burst models for a 9-million-year-old population yield SFRs that are 57% higher than those given in Equation 1 (Leitherer et al 1995b).

It is important when using this method to apply an SFR calibration that is appropriate to the population of interest.

The main advantages of this technique are that it is directly tied to the photospheric emission of the young stellar population and it can be applied to star-forming galaxies over a wide range of redshifts. As a result, it is currently the most powerful probe of the cosmological evolution in the SFR (Madau et al 1996, Ellis 1997). The chief drawbacks of the method are its sensitivity to extinction and the form of the IMF. Typical extinction corrections in the integrated UV magnitudes are 0–3 magnitudes (mag) (Buat 1992, Buat & Xu 1996). The spatial distribution of the extinction is very patchy, with the emergent UV emission dominated by regions of relatively low obscuration (Calzetti et al 1994), so calibrating the extinction correction is problematic. The best determinations are based on two-component radiative transfer models, which take into account the clumpy distribution of dust and make use of reddening information from the Balmer decrement or IR recombination lines (e.g. Buat 1992, Calzetti et al 1994, Buat & Xu 1996, Calzetti 1997).

The other main limitation, which is shared by all of the direct methods, is the dependence of the derived SFRs on the assumed form of the IMF. The integrated spectrum in the 1500- to 2500-Å range is dominated by stars with masses above $\sim 5 M_{\odot}$, so the SFR determination involves a large extrapolation to lower stellar masses. Fortunately, there is little evidence for large systematic variations in the IMF among star-forming galaxies (Scalo 1986, Gilmore et al 1998), with the possible exception of IR-luminous starbursts, where the UV emission is of little use anyway.

2.3 *Recombination Lines*

Figure 1 shows that the most dramatic change in the integrated spectrum with galaxy type is a rapid increase in the strengths of the nebular emission lines. The nebular lines effectively re-emit the integrated stellar luminosity of galaxies shortward of the Lyman limit, so they provide a direct, sensitive probe of the young massive stellar population. Most applications of this method have been based on measurements of the $H\alpha$ line, but other recombination lines, including $H\beta$, $P\alpha$, $P\beta$, $Br\alpha$, and $Br\gamma$, have been used as well.

The conversion factor between ionizing flux and the SFR is usually computed using an evolutionary synthesis model. Only stars with masses of $>10 M_{\odot}$ and lifetimes of <20 Myr contribute significantly to the integrated ionizing flux, so the emission lines provide a nearly instantaneous measure of the SFR, independent of the previous star formation history. Calibrations have been published by numerous authors, including Kennicutt (1983a), Gallagher et al (1984), Kennicutt et al (1994), Leitherer & Heckman (1995), and Madau et al (1998). For solar abundances and the same Salpeter IMF (0.1–100 M_{\odot}) as was used in

deriving Equation 1, the calibrations of Kennicutt et al (1994) and Madau et al (1998) yield

$$\begin{aligned} \text{SFR}(M_{\odot} \text{ year}^{-1}) &= 7.9 \times 10^{-42} L(\text{H}\alpha) \text{ (ergs s}^{-1}\text{)} \\ &= 1.08 \times 10^{-53} Q(H^0) \text{ (s}^{-1}\text{)}, \end{aligned} \quad (2)$$

where $Q(H^0)$ is the ionizing photon luminosity and the $\text{H}\alpha$ calibration is computed for Case B recombination at $T_e = 10,000$ K. The corresponding conversion factor for $L(\text{Br}\gamma)$ is 8.2×10^{-40} in the same units, and it is straightforward to derive conversions for other recombination lines. Equation 2 yields SFRs that are 7% lower than the widely used calibration of Kennicutt (1983a), with the difference reflecting a combination of updated stellar models and a slightly different IMF (Kennicutt et al 1994). As with other methods, there is a significant variation among published calibrations ($\sim 30\%$), with most of the dispersion reflecting differences in the stellar evolution and atmosphere models.

Large $\text{H}\alpha$ surveys of normal galaxies have been published by Cohen (1976), Kennicutt & Kent (1983), Romanishin (1990), Gavazzi et al (1991), Ryder & Dopita (1994), Gallego et al (1995), and Young et al (1996). Imaging surveys have been published by numerous other authors, with some of the largest including Hodge & Kennicutt (1983), Hunter & Gallagher (1985), Ryder & Dopita (1993), Phillips (1993), Evans et al (1996), González Delgado et al (1997), and Feinstein (1997). Gallego et al (1995) have observed a complete emission-line selected sample, in order to measure the volume-averaged SFR in the local universe, and this work has been applied extensively to studies of the evolution in the SFR density of the universe (Madau et al 1996).

The primary advantages of this method are its high sensitivity and the direct coupling between the nebular emission and the massive SFR. The star formation in nearby galaxies can be mapped at high resolution even with small telescopes, and the $\text{H}\alpha$ line can be detected in the redshifted spectra of starburst galaxies to $z \gg 2$ (e.g. Bechtold et al 1997). The chief limitations of the method are its sensitivity to uncertainties in extinction and the IMF and the assumption that all of the massive star formation is traced by the ionized gas. The escape fraction of ionizing radiation from individual HII regions has been measured both directly (Oey & Kennicutt 1997) and from observations of the diffuse $\text{H}\alpha$ emission in nearby galaxies (e.g. Hunter et al 1993, Walterbos & Braun 1994, Kennicutt et al 1995, Ferguson et al 1996, Martin 1997), with fractions of 15–50% derived in both sets of studies. Thus it is important when using this method to include the diffuse $\text{H}\alpha$ emission in the SFR measurement (Ferguson et al 1996). However, the escape fraction from a galaxy as a whole should be much lower. Leitherer et al (1995a) directly measured the redshifted Lyman continuum region in four starburst galaxies, and they derived an upper limit of 3% on the escape

fraction of ionizing photons. Much higher global escape fractions of 50–94% and local escape fractions as high as 99% have been estimated by Patel & Wilson (1995a,b), based on a comparison of O-star densities and $H\alpha$ luminosities in M33 and NGC 6822, but those results are subject to large uncertainties because the O-star properties and SFRs were derived from *UBV* photometry, without spectroscopic identifications. If the direct limit of <3% from Leitherer et al (1995a) is representative, then density bounding effects are a negligible source of error in this method. However, it is very important to test this conclusion by extending these types of measurements to a more diverse sample of galaxies.

Extinction is probably the most important source of systematic error in $H\alpha$ -derived SFRs. The extinction can be measured by comparing $H\alpha$ fluxes with those of IR recombination lines or the thermal radio continuum. Kennicutt (1983a) and Niklas et al (1997) have used integrated $H\alpha$ and radio fluxes of galaxies to derive a mean extinction $A(H\alpha) = 0.8\text{--}1.1$ mag. Studies of large samples of individual HII regions in nearby galaxies yield similar results, with mean $A(H\alpha) = 0.5\text{--}1.8$ mag (e.g. Caplan & Deharveng 1986, Kaufman et al 1987, van der Hulst et al 1988, Caplan et al 1996).

Much higher extinction is encountered in localized regions, especially in the the dense HII regions in circumnuclear starbursts, and there the near-IR Paschen or Brackett recombination lines are required to reliably measure the SFR. Compilations of these data include those by Puxley et al (1990), Ho et al (1990), Calzetti et al (1996), Goldader et al (1995, 1997), Engelbracht (1997), and references therein. The Paschen and Brackett lines are typically 1–2 orders of magnitude weaker than $H\alpha$, so most measurements to date have been restricted to high surface brightness nuclear HII regions, but it is gradually becoming feasible to extend this approach to galaxies as a whole. The same method can be applied to higher-order recombination lines or the thermal continuum emission at submillimeter and radio wavelengths. Examples of such applications include $H53\alpha$ measurements of M82 by Puxley et al (1989) and radio continuum measurements of disk galaxies and starbursts by Israel & van der Hulst (1983), Klein & Grave (1986), Turner & Ho (1994), and Niklas et al (1995).

The ionizing flux is produced almost exclusively by stars with $M > 10 M_{\odot}$, so SFRs derived from this method are especially sensitive to the form of the IMF. Adopting the Scalo (1986) IMF, for example, yields SFRs that are approximately three times higher than that derived with a Salpeter IMF. Fortunately, the $H\alpha$ equivalent widths and broadband colors of galaxies are very sensitive to the slope of the IMF over the mass range 1–30 M_{\odot} , and these can be used to constrain the IMF slope (Kennicutt 1983a, Kennicutt et al 1994). The properties of normal disks are well fitted by a Salpeter IMF (or by a Scalo function with Salpeter slope above 1 M_{\odot}), consistent with observations of resolved stellar populations in nearby galaxies (e.g. Massey 1998). As with the UV continuum

method, it is important when applying published SFRs to take proper account of the IMF that was assumed.

2.4 *Forbidden Lines*

The $H\alpha$ emission line is redshifted out of the visible window beyond $z \sim 0.5$, so there is considerable interest in calibrating bluer emission lines as quantitative SFR tracers. Unfortunately, the integrated strengths of $H\beta$ and the higher order Balmer emission lines are poor SFR diagnostics because the lines are weak and stellar absorption more strongly influences the emission-line fluxes. These lines, in fact, are rarely seen in emission at all in the integrated spectra of galaxies earlier than Sc (Kennicutt 1992a; also see Figure 1).

The strongest emission feature in the blue is the $[\text{OII}]\lambda 3727$ forbidden-line doublet. The luminosities of forbidden lines are not directly coupled to the ionizing luminosity, and their excitation is sensitive to abundance and the ionization state of the gas. However, the excitation of $[\text{OII}]$ is sufficiently well behaved that it can be calibrated empirically (through $H\alpha$) as a quantitative SFR tracer. Even this indirect calibration is extremely useful for lookback studies of distant galaxies because $[\text{OII}]$ can be observed in the visible out to redshifts $z \sim 1.6$, and it has been measured in several large samples of faint galaxies (Cowie et al 1996, 1997; Ellis 1997, and references therein).

Calibrations of SFRs in terms of $[\text{OII}]$ luminosity have been published by Gallagher et al (1989), based on large-aperture spectrophotometry of 75 blue irregular galaxies, and by Kennicutt (1992a), using integrated spectrophotometry of 90 normal and peculiar galaxies. When converted to the same IMF and $H\alpha$ calibration, the resulting SFR scales differ by a factor of 1.57, reflecting excitation differences in the two samples. Adopting the average of these calibrations yields

$$\text{SFR}(M_{\odot} \text{ year}^{-1}) = (1.4 \pm 0.4) \times 10^{-41} L[\text{OII}] \text{ (ergs s}^{-1}\text{)}, \quad (3)$$

where the uncertainty indicates the range between blue emission-line galaxies (lower limit) and samples of more luminous spiral and irregular galaxies (upper limit). As with Equations 1 and 2, the observed luminosities must be corrected for extinction, in this case the extinction at $H\alpha$, because of the manner in which the $[\text{OII}]$ fluxes were calibrated.

The SFRs derived from $[\text{OII}]$ are less precise than those from $H\alpha$ because the mean $[\text{OII}]/H\alpha$ ratios in individual galaxies vary considerably, over 0.5–1.0 dex in Gallagher et al's (1989) and Kennicutt's (1992a) samples, respectively. The $[\text{OII}]$ -derived SFRs may also be prone to systematic errors from extinction and variations in the diffuse gas fraction. The excitation of $[\text{OII}]$ is especially high in the diffuse ionized gas in starburst galaxies (Hunter & Gallagher 1990, Hunter

1994, Martin 1997), enough to more than double the $L[\text{OII}]/\text{SFR}$ ratio in the integrated spectrum (Kennicutt 1992a). On the other hand, metal abundance has a relatively small effect on the $[\text{OII}]$ calibration, over most of the abundance range of interest ($0.05 Z_{\odot} \leq Z \leq 1 Z_{\odot}$). Overall the $[\text{OII}]$ lines provide a very useful estimate of the systematics of SFRs in samples of distant galaxies, and they are especially useful as a consistency check on SFRs derived in other ways.

2.5 *Far-Infrared Continuum*

A significant fraction of the bolometric luminosity of a galaxy is absorbed by interstellar dust and re-emitted in the thermal IR, at wavelengths of roughly 10–300 μm . The absorption cross section of the dust is strongly peaked in the ultraviolet, so in principle the FIR emission can be a sensitive tracer of the young stellar population and SFR. The IRAS survey provides FIR fluxes for over 30,000 galaxies (Moshir et al 1992), offering a rich reward to those who can calibrate an accurate SFR scale from the 10- to 100- μm FIR emission.

The efficacy of the FIR luminosity as an SFR tracer depends on the contribution of young stars to heating of the dust and on the optical depth of the dust in the star forming regions. The simplest physical situation is one in which young stars dominate the radiation field throughout the UV–visible and the dust opacity is high everywhere, in which case the FIR luminosity measures the bolometric luminosity of the starburst. In such a limiting case the FIR luminosity is the ultimate SFR tracer, providing what is essentially a calorimetric measure of the SFR. Such conditions roughly hold in the dense circumnuclear starbursts that power many IR-luminous galaxies.

The physical situation is more complex in the disks of normal galaxies, however (e.g. Lonsdale & Helou 1987, Cox & Mezger 1989, Rowan-Robinson & Crawford 1989). The FIR spectra of galaxies contain both a “warm” component associated with dust around young star-forming regions ($\bar{\lambda} \sim 60 \mu\text{m}$) and a cooler “infrared cirrus” component ($\bar{\lambda} \geq 100 \mu\text{m}$), which is associated with more extended dust heated by the interstellar radiation field. In blue galaxies, both spectral components may be dominated by young stars, but in red galaxies, where the composite stellar continuum drops off steeply in the blue, dust heating from the visible spectra of older stars may be very important.

The relation of the global FIR emission of galaxies to the SFR has been a controversial subject. In late-type star-forming galaxies, where dust heating from young stars is expected to dominate the 40- to 120- μm emission, the FIR luminosity correlates with other SFR tracers such as the UV continuum and $\text{H}\alpha$ luminosities (e.g. Lonsdale & Helou 1987, Sauvage & Thuan 1992, Buat & Xu 1996). However, early-type (S0–Sab) galaxies often exhibit high FIR luminosities but much cooler, cirrus-dominated emission. This emission has

usually been attributed to dust heating from the general stellar radiation field, including the visible radiation from older stars (Lonsdale & Helou 1987, Buat & Deharveng 1988, Rowan-Robinson & Crawford 1989, Sauvage & Thuan 1992, 1994, Walterbos & Greenawalt 1996). This interpretation is supported by anomalously low UV and $H\alpha$ emission (relative to the FIR luminosity) in these galaxies. However, Devereux & Young (1990) and Devereux & Hameed (1997) have argued that young stars dominate the 40- to 120- μm emission in all of these galaxies, so that the FIR emission directly traces the SFR. They have provided convincing evidence that young stars are an important source of FIR luminosity in at least some early-type galaxies, including barred galaxies with strong nuclear starbursts and some unusually blue objects (Section 4). On the other hand, many early-type galaxies show no independent evidence of high SFRs, suggesting that the older stars or active galactic nuclei (AGNs) are responsible for much of the FIR emission. The *Space Infrared Telescope Facility*, scheduled for launch early in the next decade, should provide high-resolution FIR images of nearby galaxies and clarify the relationship between the SFR and IR emission in these galaxies.

The ambiguities discussed above affect the calibration of SFRs in terms of FIR luminosity, and there probably is no single calibration that applies to all galaxy types. However, the FIR emission should provide an excellent measure of the SFR in dusty circumnuclear starbursts. The SFR vs L_{FIR} conversion is derived using synthesis models as described above. In the optically thick limit, it is only necessary to model the bolometric luminosity of the stellar population. The greatest uncertainty in this case is adoption of an appropriate age for the stellar population; this may be dictated by the time scale of the starburst itself or by the time scale for the dispersal of the dust (so the $\tau \gg 1$ approximation no longer holds). Calibrations have been published by several authors under different assumptions about the star formation time scale (e.g. Hunter et al 1986, Lehnert & Heckman 1996, Meurer et al 1997, Kennicutt 1998). Applying the models of Leitherer & Heckman (1995) for continuous bursts of age 10–100 Myr and adopting the IMF in this paper yields the following relation (Kennicutt 1998):

$$\text{SFR}(M_{\odot} \text{ year}^{-1}) = 4.5 \times 10^{-44} L_{FIR} (\text{ergs s}^{-1}) \text{ (starbursts)}, \quad (4)$$

where L_{FIR} refers to the IR luminosity integrated over the full-, mid-, and far-IR spectrum (8–1000 μm), though for starbursts most of this emission will fall in the 10- to 120- μm region (readers should beware that the definition of L_{FIR} varies in the literature). Most of the other published calibrations lie within $\pm 30\%$ of Equation 4. Strictly speaking, the relation given above applies only to starbursts with ages less than 10^8 years, where the approximations applied are valid. In more quiescent, normal star-forming galaxies, the relation will be

more complicated; the contribution of dust heating from old stars will tend to lower the effective coefficient in Equation 4, whereas the lower optical depth of the dust will tend to increase the coefficient. In such cases, it is probably better to rely on an empirical calibration of $\text{SFR}/L_{\text{FIR}}$ that is based on other methods. For example, Buat & Xu (1996) derived a coefficient of $8_{-3}^{+8} \times 10^{-44}$, valid for galaxies of type Sb and later only, based on IRAS and UV flux measurements of 152 disk galaxies. The FIR luminosities share the same IMF sensitivity as the other direct star formation tracers, and it is important to be consistent when comparing results from different sources.

3. DISK STAR FORMATION

The techniques described above have been used to measure SFRs in hundreds of nearby galaxies, and these have enabled us to delineate the main trends in SFRs and star formation histories along the Hubble sequence. Although it is customary to analyze the integrated SFRs of galaxies, taken as a whole, large-scale star formation takes place in two very distinct physical environments: one in the extended disks of spiral and irregular galaxies; the other in compact, dense gas disks in the centers of galaxies. Both regimes are significant contributors to the total star formation in the local universe, but they are traced at different wavelengths and follow completely different patterns along the Hubble sequence. Consequently, I discuss the disk and circumnuclear star formation properties of galaxies separately.

3.1 *Global Star Formation Rates Along the Hubble Sequence*

Comprehensive analyses of the global SFRs of galaxies have been carried out using $\text{H}\alpha$ surveys (Kennicutt 1983a, Gallagher et al 1984, Caldwell et al 1991, 1994, Kennicutt et al 1994, Young et al 1996), UV continuum surveys (Donas et al 1987, Deharveng et al 1994), FIR data (Sauvage & Thuan 1992, Walterbos & Greenawalt 1996, Tomita et al 1996, Devereux & Hameed 1997), and multi-wavelength surveys (Gavazzi & Scodreggio 1996, Gavazzi et al 1996). The absolute SFRs in galaxies, expressed in terms of the total mass of stars formed per year, show an enormous range, from virtually zero in gas-poor elliptical, S0, and dwarf galaxies to $\sim 20 M_{\odot} \text{ year}^{-1}$ in gas-rich spirals. Much larger global SFRs, up to $\sim 100 M_{\odot} \text{ year}^{-1}$, can be found in optically selected starburst galaxies, and SFRs as high as $1000 M_{\odot} \text{ year}^{-1}$ may be reached in the most luminous IR starburst galaxies (Section 4). The highest SFRs are associated almost uniquely with strong tidal interactions and mergers.

Part of the large dynamic range in absolute SFRs simply reflects the enormous range in galaxy masses, so it is more illuminating to examine the range in

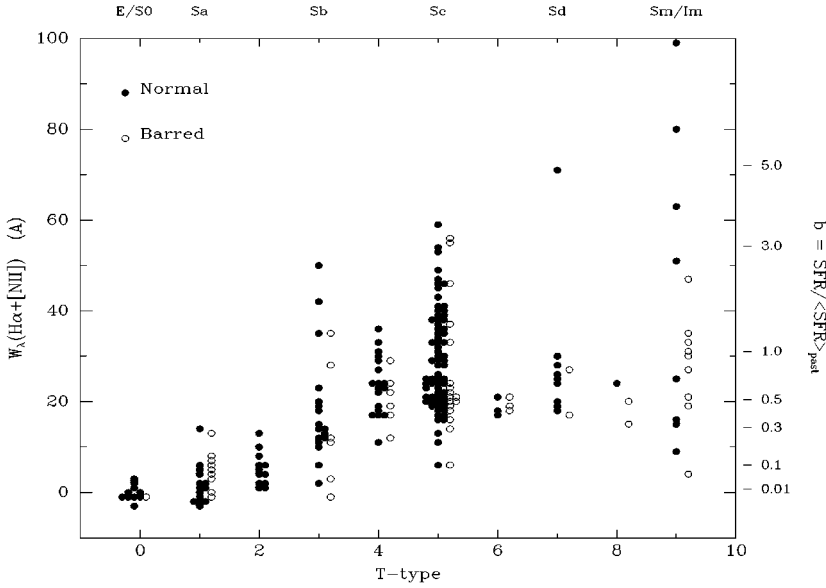


Figure 3 Distribution of integrated $H\alpha + [NII]$ emission-line equivalent widths for a large sample of nearby spiral galaxies, subdivided by Hubble type and bar morphology. The *right axis scale* shows corresponding values of the stellar birthrate parameter b , which is the ratio of the present SFR to that averaged over the past, as described in Section 5.1.

relative SFRs, normalized per unit mass or luminosity. This is illustrated in Figure 3, which shows the distribution of $H\alpha + [NII]$ equivalent widths (EWs) in a sample of 227 nearby bright galaxies ($B_T < 13$), subdivided by Hubble type. The data were taken from the photometric surveys of Kennicutt & Kent (1983) and Romanishin (1990). The measurements include the $H\alpha$ and the neighboring $[NII]$ lines; corrections for $[NII]$ contamination are applied when determining the SFRs. The EW is defined as the emission-line luminosity normalized to the adjacent continuum flux, and hence it is a measure of the SFR per unit (red) luminosity.

Figure 3 shows a range of more than two orders of magnitude in the SFR per unit luminosity. The EWs show a strong dependence on Hubble type, increasing from zero in E/S0 galaxies (within the observational errors) to 20–150 Å in late-type spiral and irregular galaxies. When expressed in terms of absolute SFRs, this corresponds to a range of 0–10 $M_{\odot} \text{ year}^{-1}$ for an L^* galaxy (roughly comparable in luminosity to the Milky Way). The SFR measured in this way increases by approximately a factor of 20 between types Sa and Sc (Caldwell

et al 1991, Kennicutt et al 1994). SFRs derived from the UV continuum and broadband visible colors show comparable behavior (e.g. Larson & Tinsley 1978, Donas et al 1987, Buat et al 1989, Deharveng et al 1994).

High-resolution imaging of individual galaxies reveals that the changes in the disk SFR along the Hubble sequence are produced in roughly equal parts by an increase in the total number of star-forming regions per unit mass or area and by an increase in the characteristic masses of individual regions (Kennicutt et al 1989a, Caldwell et al 1991, Bresolin & Kennicutt 1997). These trends are seen both in the $H\alpha$ luminosities of the HII regions as well as in the continuum luminosity functions of the embedded OB associations (Bresolin & Kennicutt 1997). A typical OB star in an Sa galaxy forms in a cluster containing only a few massive stars, whereas an average massive star in a large Sc or Irr galaxy forms in a giant HII/OB association containing hundreds or thousands of OB stars. These differences in clustering properties of the massive stars may strongly influence the structure and dynamics of the interstellar medium (ISM) along the Hubble sequence (Norman & Ikeuchi 1989, Heiles 1990).

Although there is a strong trend in the *average* SFRs with Hubble type, a dispersion of a factor of 10 is present in SFRs among galaxies of the same type. The scatter is much larger than would be expected from observational errors or extinction effects, so most of it must reflect real variations in the SFR. Several factors contribute to the SFR variations, including variations in gas content, nuclear emission, interactions, and possibly short-term variations in the SFR within individual objects. Although the absolute SFR varies considerably among spirals (types Sa and later), some level of massive star formation is always observed in deep $H\alpha$ images (Caldwell et al 1991). However, many of the earliest disk galaxies (S0–S0/a) show no detectable star formation at all. Caldwell et al (1994) obtained deep Fabry-Perot $H\alpha$ imaging of eight S0–S0/a galaxies, and detected HII regions in only three objects. The total SFRs in the latter galaxies are very low, $<0.01 M_{\odot} \text{ year}^{-1}$, and the upper limits on the other four galaxies rule out HII regions fainter than those of the Orion nebula. On the other hand, $H\alpha$ surveys of HI-rich S0 galaxies by Pogge & Eskridge (1987, 1993) reveal a higher fraction of disk and/or circumnuclear star-forming regions, emphasizing the heterogeneous star formation properties of these galaxies. Thronson et al (1989) reached similar conclusions based on an analysis of IRAS observations of S0 galaxies.

The relative SFRs can also be parametrized in terms of the mean SFR per unit disk area. This has the advantage of avoiding any effect of bulge contamination on total luminosities (which biases the EW distributions). Analyses of the SFR surface density distributions have been published by Deharveng et al (1994), based on UV continuum observations, and by Ryder (1993), Ryder & Dopita (1994), and Young et al (1996), based on $H\alpha$ observations. The average SFR

surface densities show a similar increase with Hubble type, but the magnitude of the change is noticeably weaker than is seen in SFRs per unit of luminosity (e.g. Figure 3), and the dispersion among galaxies of the same type is larger (see below). The stronger type dependence in the $H\alpha$ EWs (see Figure 3) is partly due to the effects of bulge contamination, which exaggerate the change in *disk* EWs by a factor of two between types Sa–Sc (Kennicutt et al 1994), but the change in disk EWs with type is still nearly twice as large as the comparable trend in SFR per unit area (Young et al 1996). The difference reflects the tendency for the late-type spirals to have somewhat more extended (i.e. lower surface brightness) star-forming disks than the early-type spirals, at least in these samples. This comparison demonstrates the danger in applying the term SFR too loosely when characterizing the systematic behavior of star formation across the Hubble sequence because the quantitative trends are dependent on the manner in which the SFR is defined. Generally speaking, a parameter that scales with the SFR per unit mass (e.g. the $H\alpha$ equivalent width) is most relevant to interpreting the evolutionary properties of disks, whereas the SFR per unit area is more relevant to parametrizing the dependence of the SFR on gas density in disks.

Similar comparisons can be made for the FIR properties of disk galaxies, and these show considerably weaker trends with Hubble type (Devereux & Young 1991, Tomita et al 1996, Devereux & Hameed 1997). This is illustrated in Figure 4, which shows the distributions of L_{FIR}/L_H from a sample of nearby galaxies studied by Devereux & Hameed (1997). Since the near-IR H -band luminosity is a good indicator of the total stellar mass, the L_{FIR}/L_H ratio provides an approximate measure of the FIR emission normalized to the mass of the parent galaxy. Figure 4 shows the expected trend toward stronger FIR emission with later Hubble type, but the trend is considerably weaker, in the sense that early-type galaxies show much higher FIR luminosities than would be expected given their UV-visible spectra. Comparisons of L_{FIR}/L_B distributions show almost no dependence on Hubble type at all (Isobe & Feigelson 1992, Tomita et al 1996, Devereux & Hameed 1997), but this is misleading because the B -band luminosity itself correlates with the SFR (see Figure 2).

The inconsistencies between the FIR and UV-visible properties of spiral galaxies appear to be due to a combination of effects (as mentioned in Section 2.5). In at least some early-type spirals, the strong FIR emission is produced by luminous, dusty star forming regions, usually concentrated in the central regions of barred spiral galaxies (Devereux 1987, Devereux & Hameed 1997). This exposes an important bias in the visible- and UV-based studies of SFRs in galaxies, in that they often do not take into account the substantial star formation in the dusty nuclear regions, which can dominate the global SFR in an early-type galaxy. Devereux & Hameed emphasized the importance of observing a sufficiently large and diverse sample of early-type galaxies, in order

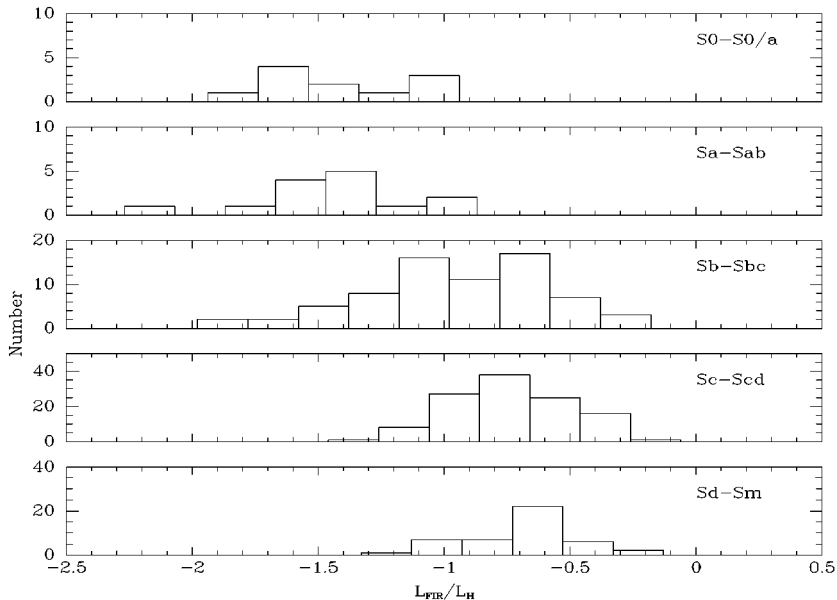


Figure 4 Distributions of 40- to 120- μm infrared (IR) luminosity for nearby galaxies, normalized to near-IR H -band luminosity, as a function of Hubble type. Adapted from Devereux & Hameed (1997), with elliptical and irregular galaxies excluded.

to fully characterize the range of star formation properties. However, it is also likely that much of the excess FIR emission in early-type spirals is unrelated to star formation, reflecting instead the effects of dust heating from evolved stellar populations (Section 2.5). Radiative transfer modeling by Walterbos & Greenawalt (1996) demonstrates that this effect can readily account for the trends seen in Figure 4.

The interpretation in the remainder of this review is based on the SFR trends revealed by the $H\alpha$, UV continuum, broadband colors, and integrated spectra, which are consistent with a common evolutionary picture of the Hubble sequence. However, it is important to bear in mind that this picture applies only to the extended, extranuclear star formation in spiral and irregular disks. The circumnuclear star formation follows quite different patterns, as discussed in Section 4.2.

3.2 Dependence of Star Formation Rates on Gas Content

The strong trends in disk SFRs that characterize the Hubble sequence presumably arise from more fundamental relationships between the global SFR and

other physical properties of galaxies, such as their gas contents or dynamical structure. The physical regulation of the SFR is a mature subject in its own right, and a full discussion is beyond the scope of this review. However, it is very instructive to examine the global relationships between the disk-averaged SFRs and gas densities of galaxies, as they reveal important insights into the physical nature of the star formation sequence and serve to quantify the range of physical conditions and evolutionary properties of disks.

Comparisons of the large-scale SFRs and gas contents of galaxies have been carried out by several authors, most recently Buat et al (1989), Kennicutt (1989, 1998), Buat (1992), Boselli (1994), Deharveng et al (1994), and Boselli et al (1995). Figure 5 shows the relationship between the disk-averaged SFR surface density Σ_{SFR} and average total (atomic plus molecular) gas density Σ_{gas} , for a sample of 61 normal spiral galaxies with $H\alpha$, HI, and CO observations (Kennicutt 1998). The SFRs were derived from extinction-corrected $H\alpha$ fluxes,

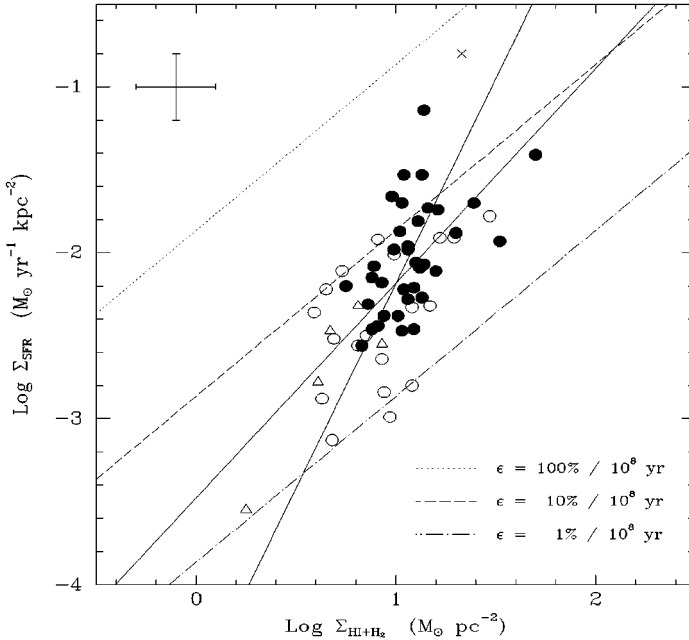


Figure 5 Correlation between disk-averaged SFR per unit area and average gas surface density, for 61 normal disk galaxies. Symbols are coded by Hubble type: Sa–Sab (open triangles); Sb–Sbc (open circles); Sc–Sd (solid points); Irr (cross). The dashed and dotted lines show lines of constant global star formation efficiency. The error bars indicate the typical uncertainties for a given galaxy, including systematic errors.

using the SFR calibration in Equation 2. The surface densities were averaged within the corrected optical radius R_o , as taken from the *Second Reference Catalog of Bright Galaxies* (de Vaucouleurs et al 1976).

Figure 5 shows that disks possess large ranges in both the mean gas density (factor of 20–30) and mean SFR surface density (factor of 100). The data points are coded by galaxy type, and they show that both the gas and SFR densities are correlated with Hubble type on average, but with large variations among galaxies of a given type. In addition, there is an underlying correlation between SFR and gas density that is largely independent of galaxy type. This shows that much of the scatter in SFRs among galaxies of the same type can be attributed to an underlying dispersion in gas contents. The data can be fitted to a Schmidt (1959) law of the form $\Sigma_{SFR} = A \Sigma_{gas}^N$. The best-fitting slope N ranges from 1.4 for a conventional least squares fit (minimizing errors in SFRs only) to $N = 2.4$ for a bivariate regression, as shown by the *solid lines* in Figure 5. Values of N in the range 0.9–1.7 have been derived by previous workers, based on SFRs derived from $H\alpha$, UV, and FIR data (Buat et al 1989, Kennicutt 1989, Buat 1992, Deharveng et al 1994). The scatter in SFRs at a given gas density is large, and most of this dispersion is probably introduced by averaging the SFRs and gas densities over a large dynamic range of local densities within the individual disks (Kennicutt 1989, 1998).

Figure 5 also contains information on the typical global efficiencies of star formation and gas consumption time scales in disks. The *dashed* and *dotted lines* indicate constant, disk-averaged efficiencies of 1, 10, and 100% per 10^8 years. The average value for these galaxies is 4.8%, meaning that the average disk converts 4.8% of its gas (within the radius of the optical disk) every 10^8 years. Since the typical gas mass fraction in these disks is about 20%, this implies that stellar mass of a disk grows by about 1% per 10^8 years, i.e. the time scale for building the disk (at the present rate) is comparable to the Hubble time. The efficiencies can also be expressed in terms of the average gas depletion time scale, which for this sample is 2.1 Gyr. Recycling of interstellar gas from stars extends the actual time scale for gas depletion by factors of 2–3 (Ostriker & Thuan 1975, Kennicutt et al 1994).

3.3 Other Global Influences on Star Formation Rate

What other global properties of a galaxy influence its SFR? It is plausible to expect the mass, bar structure, spiral arm structure, or environment to be important, and empirical information on all of these are available.

3.3.1 LUMINOSITY AND MASS Gavazzi & Scodiggio (1996) and Gavazzi et al (1996) have compiled UV, visible, and near-IR photometry for over 900 nearby galaxies, and they found an anti-correlation between the SFR per unit mass

and the galaxy luminosity, as indicated by broadband colors and $H\alpha$ EWs. At least part of this trend seems to reflect the same dependence of SFR on Hubble type discussed above, but a mass dependence is also observed among galaxies of the same Hubble type. It is interesting that there is considerable overlap between the color-luminosity relations of different spiral types, which suggests that part of the trends that are attributed to morphological type may be more fundamentally related to total mass. A strong correlation between $B - H$ color and galaxy luminosity or linewidth has been discussed previously by Tully et al (1982) and Wyse (1983). The trends seem to be especially strong for redder colors, which are more closely tied to the star formation history and mean metallicity than the current SFR. More data are needed to fully disentangle the effects of galaxy type and mass, for both the SFR and the star formation history.

3.3.2 BARS Stellar bars can strongly perturb the gas flows in disks and trigger nuclear star formation (see next section), but they do not appear to significantly affect the total disk SFRs. Figure 3 plots the $H\alpha$ EW distributions separately for normal (SA and SAB) and barred (SB) spirals, as classified in the *Second Reference Catalog of Bright Galaxies*. There is no significant difference in the EW distributions (except possibly for the Sa/SBa galaxies), which suggests that the global effect of a bar on the *disk* SFR is unimportant. Ryder & Dopita (1994) reached the same conclusion based on $H\alpha$ observations of 24 southern galaxies.

Tomita et al (1996) carried out a similar comparison of FIR emission, based on IRAS data and broadband photometry for 139 normal spirals and 260 barred Sa–Sc galaxies. They compared the distributions of L_{FIR}/L_B ratios for Sa/SBa, Sb/SBb, and Sc/SBc galaxies and concluded that there is no significant correlation with bar structure, consistent with the $H\alpha$ results. There is evidence for a slight excess in FIR emission in SBa galaxies, which could reflect bar-triggered circumnuclear star formation in some of the galaxies, though the statistical significance of the result is marginal (Tomita et al 1996).

Recent work by Martinet & Friedli (1997) suggests that influence of bars on the global SFR may not be as simple as suggested above. They analyzed $H\alpha$ and FIR-based SFRs for a sample of 32 late-type barred galaxies and found a correlation between SFR and the strength and length of the bar. This suggests that large samples are needed to study the effects of bars on the large-scale SFR and that the structural properties of the bars themselves need to be incorporated in the analysis.

3.3.3 SPIRAL ARM STRUCTURE Similar tests have been carried out to explore whether a strong grand-design spiral structure enhances the global SFR.

Elmegreen & Elmegreen (1986) compared UV and visible broadband colors and $H\alpha$ EWs for galaxies they classified as grand design (strong two-armed spiral patterns) and flocculent (ill-defined, patchy spiral arms), and they found no significant difference in SFRs. McCall & Schmidt (1986) compared the supernova rates in grand-design and flocculent spirals and drew similar conclusions. Grand-design spiral galaxies show strong local enhancements of star formation in their spiral arms (e.g. Cepa & Beckman 1990, Knapen et al 1992), so the absence of a corresponding excess in their total SFRs suggests that the primary effect of the spiral density wave is to concentrate star formation in the arms, but not to increase the global efficiency of star formation.

3.3.4 GALAXY-GALAXY INTERACTIONS Given the modest effects of internal disk structure on global SFRs, it is perhaps somewhat surprising that external environmental influences can have much stronger effects on the SFR. The most important influences by far are tidal interactions. Numerous studies of the global $H\alpha$ and FIR emission of interacting and merging galaxies have shown strong excess star formation (e.g. Bushouse 1987, Kennicutt et al 1987, Bushouse et al 1988, Telesco et al 1988, Xu & Sulentic 1991, Liu & Kennicutt 1995). The degree of the SFR enhancement is highly variable, ranging from zero in gas-poor galaxies to on the order of 10–100 times in extreme cases. The average enhancement in SFR over large samples is a factor of 2–3. Much larger enhancements are often seen in the circumnuclear regions of strongly interacting and merging systems (see next section). This subject is reviewed in depth by Kennicutt et al (1998).

3.3.5 CLUSTER ENVIRONMENT There is evidence that a cluster environment systematically alters the star formation properties of galaxies, independently of the well-known density-morphology relation (Dressler 1984). Many spiral galaxies located in rich clusters exhibit significant atomic gas deficiencies (Haynes et al 1984, Warmels 1988, Cayatte et al 1994), which presumably are the result of ram pressure stripping from the intercluster medium, combined with tidal stripping from interactions with other galaxies and the cluster potential. In extreme cases, the gas removal would be expected to affect the SFRs as well. Kennicutt (1983b) compared $H\alpha$ EWs of 26 late-type spirals in the Virgo cluster core with the field sample of Kennicutt & Kent (1983) and found evidence for a 50% lower SFR in Virgo, comparable to the level of HI deficiency. The UV observations of the cluster Abell 1367 by Donas et al (1990) also show evidence for lower SFRs. However, subsequent studies of the Coma, Cancer, and A1367 clusters by Kennicutt et al (1984) and Gavazzi et al (1991) showed no reduction in the average SFRs and, if anything, a higher number of strong emission-line galaxies.

A comprehensive $H\alpha$ survey of eight Abell clusters by Moss & Whittle (1993) suggests that the effects of cluster environment on global star formation activity are quite complex. They found a 37–46% lower $H\alpha$ detection rate among Sb, Sc, and irregular galaxies in the clusters, but a 50% higher detection rate among Sa–Sab galaxies. They argued that these results arise from a combination of competing effects, including reduced star formation from gas stripping as well as enhanced star formation triggered by tidal interactions. Ram-pressure–induced star formation may also be taking place in a few objects (Gavazzi & Jaffe 1985).

4. CIRCUMNUCLEAR STAR FORMATION AND STARBURSTS

It has been known from the early photographic work of Morgan (1958) and Sérsic & Pastoriza (1967) that the circumnuclear regions of many spiral galaxies harbor luminous star-forming regions, with properties that are largely decoupled from those of the more extended star-forming disks. Subsequent spectroscopic surveys revealed numerous examples of bright emission-line nuclei with spectra resembling those of HII regions (e.g. Heckman et al 1980, Stauffer 1982, Balzano 1983, Keel 1983). The most luminous of these were dubbed starbursts by Weedman et al (1981). The opening of the mid-IR and FIR regions fully revealed the distinctive nature of the nuclear star formation (e.g. Rieke & Low 1972, Harper & Low 1973, Rieke & Lebofsky 1978, Telesco & Harper 1980). The IRAS survey led to the discovery of large numbers of ultraluminous star-forming galaxies (Soifer et al 1987). This subject has grown into a major subfield of its own, which has been thoroughly reviewed in this series (Soifer et al 1987, Telesco 1988, Sanders & Mirabel 1996). The discussion here focuses on the range of star formation properties of the nuclear regions and the patterns in these properties along the Hubble sequence.

4.1 *Star Formation Rates and Physical Properties*

Comprehensive surveys of the star formation properties of galactic nuclei have been carried out using emission-line spectroscopy in the visible (Stauffer 1982, Keel 1983, Kennicutt et al 1989b, Ho et al 1997a,b) and mid-IR photometry (Rieke & Lebofsky 1978, Scoville et al 1983, Devereux et al 1987, Devereux 1987, Giuricin et al 1994). Nuclear emission spectra with HII region–like line ratios are found in 42% of bright spirals ($B_T < 12.5$), with the fraction increasing from 8% in S0 galaxies (and virtually zero in elliptical galaxies) to 80% in Sc–Im galaxies (Ho et al 1997a). These fractions are lower limits, especially in early-type spirals, because the star formation often is masked by a LINER or Seyfert nucleus. Similar detection fractions are found in 10- μm

surveys of optically selected spiral galaxies, but with a stronger weighting toward early Hubble types. The nuclear SFRs implied by the $H\alpha$ and IR fluxes span a large range, from a lower detection limit of $\sim 10^{-4} M_{\odot} \text{ year}^{-1}$ to well over $100 M_{\odot} \text{ year}^{-1}$ in the most luminous IR galaxies.

The physical character of the nuclear star-forming regions changes dramatically over this spectrum of SFRs. The nuclear SFRs in most galaxies are quite modest, averaging $\sim 0.1 M_{\odot} \text{ year}^{-1}$ (median $0.02 M_{\odot} \text{ year}^{-1}$) in the $H\alpha$ sample of Ho et al (1997a) and $\sim 0.2 M_{\odot} \text{ year}^{-1}$ in the (optically selected) $10\text{-}\mu\text{m}$ samples of Scoville et al (1983) and Devereux et al (1987). Given the different selection criteria and completeness levels in these surveys, the SFRs are reasonably consistent with each other, and this suggests that the nuclear star formation at the low end of the SFR spectrum typically occurs in moderately obscured regions ($A_{H\alpha} \sim 0\text{--}3$ mag) that are not physically dissimilar from normal disk HII regions (Kennicutt et al 1989b, Ho et al 1997a).

However, the IR observations also reveal a population of more luminous regions, with $L_{FIR} \sim 10^{10}\text{--}10^{13} L_{\odot}$, and corresponding SFRs on the order of $1\text{--}1000 M_{\odot} \text{ year}^{-1}$ (Rieke & Low 1972, Scoville et al 1983, Joseph & Wright 1985, Devereux 1987). Such high SFRs are not seen in optically selected samples, mainly because the luminous starbursts are uniquely associated with dense molecular gas disks (Young & Scoville 1991 and references therein), and for normal gas-to-dust ratios, one expects visible extinctions of several magnitudes or higher. The remainder of this section focuses on these luminous nuclear starbursts because they represent a star formation regime that is distinct from the more extended star formation in disks and because these bursts often dominate the total SFRs in their parent galaxies.

The IRAS all-sky survey provided the first comprehensive picture of this upper extreme in the SFR spectrum. Figure 6 shows a comparison of the total 8- to $1000\text{-}\mu\text{m}$ luminosities (as derived from IRAS) and total molecular gas masses for 87 bright IR-luminous galaxies, taken from the surveys of Tinney et al (1990) and Sanders et al (1991). Tinney et al's sample (*open circles*) includes many luminous but otherwise normal star-forming galaxies, while Sanders et al's brighter sample (*solid points*) mainly comprises starburst galaxies and a few AGNs. Strictly speaking, these measurements cannot be applied to infer the nuclear SFRs of the galaxies because they are low-resolution measurements and the samples are heterogeneous. However, circumnuclear star formation sufficiently dominates the properties of the luminous IR galaxies (e.g. Veilleux et al 1995, Lutz et al 1996) that Figure 6 (*solid points*) provides a representative indication of the range of SFRs in these IRAS-selected samples.

The most distinctive feature in Figure 6 is the range of IR luminosities. The lower range overlaps with the luminosity function of normal galaxies (the lower limit of $10^{10} L_{\odot}$ is the sample definition cutoff), but the population

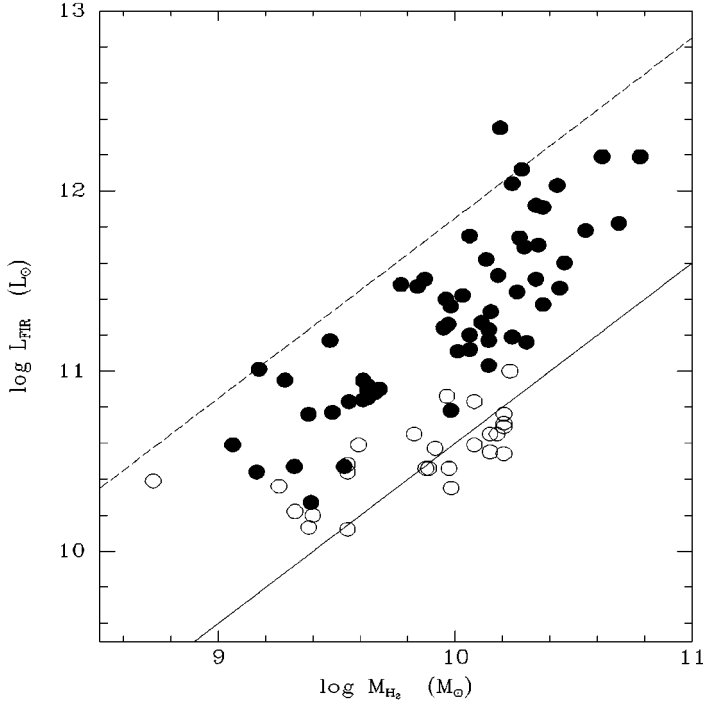


Figure 6 Relationship between integrated far-infrared (FIR) luminosity and molecular gas mass for bright IR galaxies, from Tinney et al (1990; *open circles*) and a more luminous sample by Sanders et al (1991; *solid points*). The *solid line* shows the typical L/M ratio for galaxies similar to the Milky Way. The *dashed line* shows the approximate limiting luminosity for a galaxy forming stars with 100% efficiency on a dynamic time scale, as described in the text.

of IR galaxies extends upward to $>10^{12.5} L_{\odot}$. This would imply SFRs of up to $500 M_{\odot} \text{ year}^{-1}$ (Equation 4) if starbursts are primarily responsible for the dust heating, about 20 times larger than the highest SFRs observed in normal galaxies. Figure 6 also shows that the luminous IR galaxies are associated with unusually high molecular gas masses, which partly accounts for the high SFRs. However the typical SFR per unit gas mass is much higher than in normal disks; the *solid line* in Figure 6 shows the typical L/M ratio for normal galaxies, and the efficiencies in the IR galaxies are higher by factors of 2–30 (Young et al 1986, Solomon & Sage 1988, Sanders et al 1991). The H_2 masses used here have been derived using a standard Galactic H_2/CO conversion ratio, and if the actual conversion factor in the IRAS galaxies is lower, as is suggested by several lines of evidence, the contrast in star formation efficiencies would be even larger (e.g. Downes et al 1993, Aalto et al 1994, Solomon et al 1997).

High-resolution IR photometry and imaging of the luminous IR galaxies reveals that the bulk of the luminosity originates in compact circumnuclear regions (e.g. Wright et al 1988, Carico et al 1990, Telesco et al 1993, Smith & Harvey 1996, and references therein). Likewise, CO interferometric observations show that a large fraction of the molecular gas is concentrated in central disks, with typical radii on the order of 0.1–1 kpc and implied surface densities on the order of 10^2 – $10^5 M_{\odot} \text{pc}^{-2}$ (Young & Scoville 1991, Scoville et al 1994, Sanders & Mirabel 1996). Less massive disks with similar gas and SFR surface densities are associated with the IR-bright nuclei of spiral galaxies (e.g. Young & Scoville 1991, Telesco et al 1993, Scoville et al 1994, Smith & Harvey 1996, Rubin et al 1997). The full spectrum of nuclear starburst regions is considered in the remainder of this section.

The physical conditions in the circumnuclear star-forming disks are distinct in many respects from the more extended star-forming disks of spiral galaxies, as is summarized in Table 1. The circumnuclear star formation is especially distinctive in terms of the absolute range in SFRs, the much higher spatial concentrations of gas and stars, its burst-like nature (in luminous systems), and its systematic variation with galaxy type.

The different range of physical conditions in the nuclear starbursts is clearly seen in Figure 7, which plots the average SFR surface densities and mean molecular surface densities for the circumnuclear disks of 36 IR-selected starbursts (Kennicutt 1998). The comparison is identical to the SFR–density plot

Table 1 Star formation in disks and nuclei of galaxies

Property	Spiral disks	Circumnuclear regions
Radius	1–30 kpc	0.2–2 kpc
Star formation rate (SFR)	0–20 $M_{\odot} \text{year}^{-1}$	0–1000 $M_{\odot} \text{year}^{-1}$
Bolometric luminosity	10^6 – $10^{11} L_{\odot}$	10^6 – $10^{13} L_{\odot}$
Gas mass	10^8 – $10^{11} M_{\odot}$	10^6 – $10^{11} M_{\odot}$
Star formation time scale	1–50 Gyr	0.1–1 Gyr
Gas density	1–100 $M_{\odot} \text{pc}^{-2}$	10^2 – $10^5 M_{\odot} \text{pc}^{-2}$
Optical depth (0.5 μm)	0–2	1–1000
SFR density	0–0.1 $M_{\odot} \text{year}^{-1} \text{kpc}^{-2}$	1–1000 $M_{\odot} \text{year}^{-1} \text{kpc}^{-2}$
Dominant mode	steady state	steady state + burst
Type dependence?	strong	weak/none
Bar dependence?	weak/none	strong
Spiral structure dependence?	weak/none	weak/none
Interactions dependence?	moderate	strong
Cluster dependence?	moderate/weak	?
Redshift dependence?	strong	?

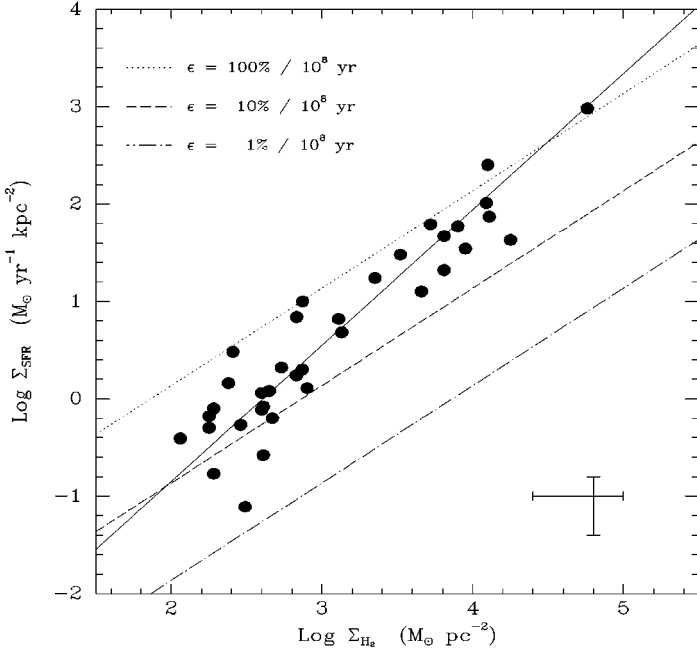


Figure 7 Correlation between disk-averaged SFR per unit area and average gas surface density, for 36 IR-selected circumnuclear starbursts. See Figure 5 for a similar comparison for normal spiral disks. The *dashed* and *dotted* lines show lines of constant star formation conversion efficiency, with the same notation as in Figure 5. The *error bars* indicate the typical uncertainties for a given galaxy, including systematic errors.

for spiral disks in Figure 5, except that in this case the SFRs are derived from FIR luminosities (Equation 4), and only molecular gas densities are plotted. HI observations show that the atomic gas fractions in these regions are on the order of only a few percent and can be safely neglected (Sanders & Mirabel 1996). The SFRs and densities have been averaged over the radius of the circumnuclear disk, as measured from high-resolution CO or IR maps, as described by Kennicutt (1998).

Figure 7 shows that the surface densities of gas and star formation in the nuclear starbursts are 1–4 orders of magnitude higher than in spiral disks overall. Densities of this order can be found in large molecular cloud complexes within spiral disks, of course, but the physical conditions in many of the nuclear starbursts are extraordinary even by those standards. For example, the typical mean densities of the largest molecular cloud complexes in M31, M33, and M51 are in the range of 40–500 $M_{\odot} \text{ pc}^{-2}$, which corresponds to the lower range of

densities in Figure 7 (Kennicutt 1998). Likewise, the SFR surface densities in the 30 Doradus giant HII region, the most luminous complex in the Local Group, reaches $100 M_{\odot} \text{ year}^{-1} \text{ kpc}^{-2}$ only in the central 10-pc core cluster. The corresponding densities in many of the starbursts exceed these values, over regions as large as a kiloparsec in radius.

The starbursts follow a relatively well-defined Schmidt law, with index $N \sim 1.4$. The nature of the star formation law is discussed further in Section 5, where we examine the SFR vs gas density relation for all of the data taken together. Figure 7 also shows that the characteristic star formation efficiencies and time scales are quite different in the starbursts. The mean conversion efficiency is 30% per 10^8 years, six times larger than in the spiral disks. Likewise, the gas consumption time scale is six times shorter, about 0.3 Gyr on average. This is hardly surprising—these objects are starbursts by definition—but Figure 7 serves to quantify the characteristic time scales for the starbursts.

As pointed out by Heckman (1994) and Lehnert & Heckman (1996), the luminous IR galaxies lie close to the limiting luminosity allowed by stellar energy generation, for a system that converts all of its gas to stars over a dynamical time scale. For a galaxy with dimensions comparable to the Milky Way, the minimum time scale for feeding the central starburst is $\sim 10^8$ years; this is also consistent with the minimum gas consumption time scale in Figure 7. At the limit of 100% star formation efficiency over this time scale, the corresponding SFR is trivially

$$\text{SFR}_{max} = 100 M_{\odot} \text{ year}^{-1} \left(\frac{M_{gas}}{10^{10} M_{\odot}} \right) \left(\frac{\tau_{gas}}{10^8 \text{ years}} \right)^{-1}. \quad (5)$$

The corresponding maximum bolometric luminosity can be estimated using Equation 4, or by calculating the maximum nuclear energy release possible from stars over 10^8 years. The latter is $\sim 0.01 \epsilon \dot{m} c^2$, where \dot{m} in this case is the SFR, and ϵ is the fraction of the total stellar mass that is burned in 10^8 years. A reasonable value of ϵ for a Salpeter IMF is about 0.05; it could be as high as 0.2 if the starburst IMF is depleted in low-mass stars (e.g. Rieke et al 1993). Combining these terms and assuming further that all of the bolometric luminosity is reradiated by the dust yields

$$L_{max} \sim 7 \times 10^{11} L_{\odot} \left(\frac{M_{gas}}{10^{10} M_{\odot}} \right) \left(\frac{\epsilon}{0.05} \right). \quad (6)$$

Using Equation 4 to convert the SFR to FIR luminosity gives nearly the same coefficient (6×10^{11}). This limiting L/M relation is shown by the *dashed line* in Figure 6, and it lies very close to the actual upper envelope of the luminous

IR galaxies. Given the number of assumptions that went into Equation 6, this agreement may be partly fortuitous; other physical processes, such as optical depth effects in the cloud, may also be important in defining the upper luminosity limits (e.g. Downes et al 1993). However, the main intent of this exercise is to illustrate that many of the most extreme circumnuclear starbursts lie near the physical limit for maximum SFRs in galaxies. Heckman (1994) extended this argument and derived the maximum SFR for a purely self-gravitating protogalaxy, and he showed that the most luminous IR galaxies lie close to this limit as well. Note that none of these limits apply to AGN-powered galaxies because the mass consumption requirements for a given mass are 1–2 orders of magnitude lower.

Taken together, these results reveal the extraordinary character of the most luminous IR starburst galaxies (Heckman 1994, Scoville et al 1994, Sanders & Mirabel 1996). They represent systems in which a mass of gas comparable to the entire ISM of a galaxy has been driven into a region on the order of 1 kpc in size, and this entire ISM is being formed into stars, with almost 100% efficiency, over a time scale on the order of 10^8 years. Such a catastrophic transfer of mass can only take place in a violent interaction or merger, or perhaps during the initial collapse phase of protogalaxies.

4.2 *Dependence on Type and Environment*

The star formation that takes place in the circumnuclear regions of galaxies also follows quite different patterns along the Hubble sequence, relative to the more extended star formation in disks. These distinctions are especially important in early-type galaxies, where the nuclear regions often dominate the global star formation in their parent galaxies.

4.2.1 HUBBLE TYPE In contrast to the extended star formation in disks, which varies dramatically along the Hubble sequence, circumnuclear star formation is largely decoupled with Hubble type. Stauffer (1982), Keel (1983), and Ho et al (1997a) investigated the dependence of nuclear $H\alpha$ emission in star forming nuclei as a function of galaxy type. The detection frequency of HII region nuclei is a strong monotonic function of type, increasing from 0% in elliptical galaxies to 8% in SO, 22% in Sa, 51% in Sb, and 80% in Sc–Im galaxies (Ho et al 1997a), though these fractions may be influenced somewhat by AGN contamination. Among the galaxies with nuclear star formation, the $H\alpha$ luminosities show the opposite trend; the average extinction-corrected luminosity of HII region nuclei in S0–Sbc galaxies is nine times higher than in Sc galaxies (Ho et al 1997a). Thus the bulk of the total nuclear star formation in galaxies is weighted toward the earlier Hubble types, even though the frequency of occurrence is higher in the late types.

Similar trends are observed in 10- μm surveys of nearby galaxies (Rieke & Lebofsky 1978, Scoville et al 1983, Devereux 1987, Devereux et al 1987, Giuricin et al 1994). Interpreting the trends in nuclear 10- μm luminosities by themselves is less straightforward because the dust can be heated by active nuclei as well as by star formation, but one can reduce this problem by excluding known AGNs from the statistics. Devereux et al (1987) analyzed the properties of an optically selected sample of 191 bright spirals, chosen to lie within or near the distance of the Virgo cluster, and found that the average nuclear 10- μm flux was virtually independent of type and, if anything, decreased by 25–30% from types Sa–Sbc to Sc–Scd. An analysis of a larger sample by Giuricin et al (1994) shows that among galaxies with HII region nuclei (as classified from optical spectra), Sa–Sb nuclei are 1.7 times more luminous at 10 μm than Sc galaxies. By contrast, the disk SFRs are typically 5–10 times lower in the early-type spirals, so the fractional contribution of the nuclei to the total SFR increases dramatically in the early-type spirals. The nuclear SFRs in some early-type galaxies are comparable to the *integrated* SFRs of late-type spirals (e.g. Devereux 1987, Devereux & Hameed 1997). Thus while luminous nuclear starbursts may occur across the entire range of spiral host types (e.g. Rieke & Lebofsky 1978, Devereux 1987), the relative effect is much stronger for the early-type galaxies; most of the star formation in these galaxies occurs in the circumnuclear regions. Clearly the physical mechanisms that trigger these nuclear outbursts are largely decoupled from the global gas contents and SFRs of their parent galaxies.

4.2.2 BAR STRUCTURE These same surveys show that nuclear star formation is strongly correlated with the presence of strong stellar bars in the parent galaxy. The first quantitative evidence came from the photographic work of Sérsic & Pastoriza (1967), who showed that 24% of nearby SB and SAB galaxies possessed detectable circumnuclear “hotspot” regions, now known to be bright HII regions and stellar associations. In contrast, none of the nonbarred galaxies studied showed evidence for hotspots. This work was followed up by Phillips (1993), who showed that the hotspots are found preferentially in early-type barred galaxies, a tendency noted already by Sérsic & Pastoriza.

The effects of bars on the H α emission from HII region nuclei have been analyzed by Ho et al (1997b). They found that the incidence of nuclear star formation is higher among the barred galaxies, but the difference is marginally significant and no excess is seen among early-type barred galaxies. However, the distributions of H α luminosities are markedly different, with the barred galaxies showing an extended tail of bright nuclei that is absent in samples of nonbarred galaxies. This tail extends over a range in H α luminosities of 3–100 $\times 10^{40}$ ergs s $^{-1}$, which corresponds to SFRs in the range 0.2–8 M_{\odot} year $^{-1}$. This tail is especially strong in the early-type barred galaxies (SB0/a–SBbc), where $\sim 30\%$ of the star forming nuclei have luminosities in this range.

Bars appear to play an especially strong role in triggering the strong IR-luminous starbursts that are found in early-type spiral galaxies. Hawarden et al (1986) and Dressel (1988) found strong excess FIR emission in early-type barred spirals, based on IRAS observations, and hypothesized that this emission was associated with circumnuclear star-forming regions. This interpretation was directly confirmed by Devereux (1987), who detected strong nuclear $10\text{-}\mu\text{m}$ emission in 40% of the early-type barred spirals in his sample. Similar excesses are not seen in samples of late-type barred galaxies. These results have been confirmed in more extensive later studies by Giuricin et al (1994) and Huang et al (1996). Although early-type barred galaxies frequently harbor a bright nuclear starburst, bars are not a necessary condition for such a starburst, as shown by Pompea & Rieke (1990).

The strong association of nuclear and circumnuclear star formation with bar structure, and the virtual absence of any other dependence on morphological type, contrasts sharply with the behavior of the disk SFRs. This implies that the evolution of the circumnuclear region is largely decoupled from that of the disk at larger radii. The strong distinctions between early-type and late-type barred galaxies appear to be associated with the structural and dynamical properties of the bars. Bars in bulge-dominated, early-type spirals tend to be very strong and efficient at transporting gas from the disk into the central regions, while bars in late-type galaxies are much weaker and are predicted to be much less efficient in transporting gas (e.g. Athanassoula 1992, Friedli & Benz 1995). All of the results are consistent with a general picture in which the circumnuclear SFRs of galaxies are determined largely by the rate of gas transport into the nuclear regions.

4.2.3 GALAXY INTERACTIONS AND MERGERS Numerous observations have established a clear causal link between strong nuclear starbursts and tidal interactions and mergers of galaxies. Since this subject is reviewed in depth elsewhere (Heckman 1990, 1994, Barnes & Hernquist 1992, Sanders & Mirabel 1996 Kennicutt et al 1998), only the main results are summarized here.

The evidence for interaction-induced nuclear star formation comes from two types of studies, statistical comparisons of the SFRs in complete samples of interacting and noninteracting galaxies, and studies of the frequency of interactions and mergers among samples of luminous starburst galaxies. Keel et al (1985) and Bushouse (1986) showed that the nuclear $H\alpha$ emission in nearby samples of interacting spiral galaxies is three to four times stronger than that in a control sample of isolated spirals. Groundbased 10- to $20\text{-}\mu\text{m}$ observations of the nuclear regions of interacting and merging galaxies showed similar or stronger enhancements, depending on how the samples were selected (Lonsdale et al 1984, Cutri & McAlary 1985, Joseph & Wright 1985, Wright et al 1988). There is an enormous range of SFRs among individual objects.

Spatially resolved data also show a stronger central concentration of the star formation in strongly interacting systems (e.g. Bushouse 1987, Kennicutt et al 1987, Wright et al 1988). Thus while the interactions tend to increase the SFR throughout galaxies, the effects in the nuclear regions are stronger. This radial concentration is consistent with the predictions of numerical simulations of interacting and merging systems (Barnes & Hernquist 1992, Mihos & Hernquist 1996, Kennicutt et al 1998).

The complementary approach is to measure the frequencies of interacting systems in samples of starburst galaxies. The most complete data of this kind come from IRAS, and they show that the importance of tidal triggering is a strong function of the strength of the starburst, with the fraction of interactions increasing from 20–30% for $L_{IR} < 10^{10} L_{\odot}$ to 70–95% for $L_{IR} > 10^{12} L_{\odot}$ (Sanders et al 1988, Lawrence et al 1989, Gallimore & Keel 1993, Leech et al 1994, Sanders & Mirabel 1996). The relatively low fraction for the lower luminosity starbursts is understandable because the corresponding SFRs ($< 1 M_{\odot} \text{ year}^{-1}$) can be sustained with relatively modest gas supplies and can be fed by internal mechanisms such as a strong bar. The most luminous starbursts, on the other hand, are associated almost exclusively with strong tidal interactions and mergers. SFRs larger than $\sim 20 M_{\odot} \text{ year}^{-1}$ are rarely observed in isolated galaxies, though some possible exceptions have been identified by Leech et al (1994). In view of the enormous fueling requirements for such starbursts (Equations 5 and 6), however, it is perhaps not surprising that an event as violent as a merger is required. These results underscore the heterogeneous nature of the starburst galaxy population, and they suggest that several triggering mechanisms are involved in producing the population.

5. INTERPRETATION AND IMPLICATIONS FOR GALAXY EVOLUTION

The observations described above can be fitted together into a coherent evolutionary picture of disk galaxies and the Hubble sequence. This section summarizes the evolutionary implications of these data, taking into account the distinct patterns seen in the disks and galactic nuclei. It concludes with a discussion of the critical role of the interstellar gas supply in regulating the SFR, across the entire range of galaxy types and environments.

5.1 *Disk Evolution Along the Hubble Sequence*

The strong trends observed in the SFR per unit of luminosity along the Hubble sequence mirror underlying trends in past star formation histories of disks (Roberts 1963, Kennicutt 1983a, Gallagher et al 1984, Sandage 1986, Kennicutt et al 1994). A useful parameter for characterizing the star formation histories is the ratio of the current SFR to the past SFR averaged over the age of the

disk, denoted b by Scalo (1986). The evolutionary synthesis models discussed in Section 2 provide relations between b and the broadband colors and $H\alpha$ EWs. Figure 3 shows the distribution of b (*right axis scale*) for an $H\alpha$ -selected sample of galaxies, based on the calibration of Kennicutt et al (1994). The typical late-type spiral has formed stars at a roughly constant rate ($b \sim 1$), which is consistent with direct measurements of the stellar age distribution in the Galactic disk (e.g. Scalo 1986). By contrast, early-type spiral galaxies are characterized by rapidly declining SFRs, with $b \sim 0.01$ – 0.1 , whereas elliptical and S0 galaxies have essentially ceased forming stars ($b = 0$). Although the values of b given above are based solely on synthesis modeling of the $H\alpha$ equivalent widths, analysis of the integrated colors and spectra of disks yield similar results (e.g. Kennicutt 1983a, Gallagher et al 1984, Bruzual & Charlot 1993, Kennicutt et al 1994).

The trends in b shown in Figure 3 are based on integrated measurements, so they are affected by bulge and nuclear contamination, which bias the trends seen along the Hubble sequence. A more detailed analysis by Kennicutt et al (1994) includes corrections for bulge contamination on the $H\alpha$ EWs. The mean value of b (for the disks alone) increases from <0.07 for Sa disks to 0.3 for Sb disks and 1.0 for Sc disks. This change is much larger than the change in bulge mass fraction over the same range of galaxy types, implying that most of the variation in the integrated photometric properties of spiral galaxies is produced by changes in the star formation histories of the disks, not in the bulge-to-disk ratio. Variations in bulge-disk structure may play an important role, however, in physically driving the evolution of the disks.

As discussed earlier, this picture has been challenged by Devereux & Hameed (1997), based on the much weaker variation in FIR luminosities along the Hubble sequence. The results of the previous section provide part of the resolution to this paradox. Many early-type barred spirals harbor luminous circumnuclear starbursts, with integrated SFRs that can be as high as the disk SFRs in late-type galaxies. If this nuclear star formation is included, then the interpretation of the Hubble sequence given above is clearly oversimplistic. For that reason, it is important to delineate between the the nuclear regions and more extended disks when characterizing the evolutionary properties of galaxies. Much of the remaining difference in interpretations hinges on the nature of the FIR emission in early-type galaxies, which may not directly trace the SFR in all galaxies.

Although Figure 3 shows a strong change in the *average* star formation history with galaxy type, it also shows a large dispersion in b among galaxies of the same type. Some of this must be due to real long-term variations in star formation history, reflecting the crudeness of the Hubble classification itself. Similar ranges are seen in the gas contents (Roberts & Haynes 1994), and these correlate roughly with the SFR and b variations (Figure 5). Short-term variations in the SFR can also explain part of the dispersion in b . Nuclear starbursts

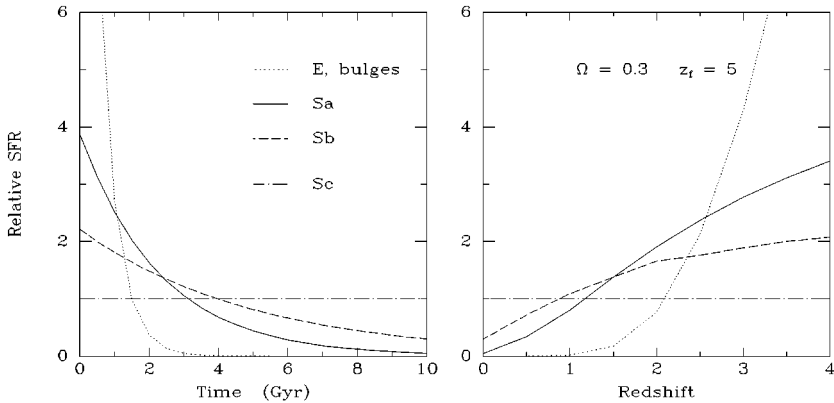


Figure 8 A schematic illustration of the evolution of the stellar birthrate for different Hubble types. The *left panel* shows the evolution of the relative SFR with time, following Sandage (1986). The curves for spiral galaxies are exponentially declining SFRs that fit the mean values of the birthrate parameter b measured by Kennicutt et al (1994). The *curve* for elliptical galaxies and bulges is an arbitrary dependence for an e-folding time of 0.5 Gyr, for comparative purposes only. The *right panel* shows the corresponding evolution in SFR with redshift, for an assumed cosmological density parameter $\Omega = 0.3$ and an assumed formation redshift $z_f = 5$.

clearly play a role in some galaxies, especially early-type barred galaxies, and interaction-induced starbursts are observed in a small percentage of nearby galaxies. Starbursts are thought to be an important, if not dominant, mode of star formation in low-mass galaxies (e.g. Hunter & Gallagher 1985, Hodge 1989, Ellis 1997), but the role of large-scale starbursts in massive galaxies is less well established (Bothun 1990, Kennicutt et al 1994, Tomita et al 1996). A definitive answer to this question will probably come from look-back studies of large samples of disk galaxies.

A schematic illustration of the trends in star formation histories is shown in Figure 8. The *left panel* compares the stellar birthrate histories of typical elliptical galaxies (and spiral bulges) and the disks of Sa, Sb, and Sc galaxies, following Sandage (1986). The curves for the spiral disks are exponential functions that correspond to the average values of b from Kennicutt et al (1994). For illustrative purposes, an exponentially declining SFR with an e-folding time scale of 0.5 Gyr is also shown, as might be appropriate for an old spheroidal population. In this simple picture, the Hubble sequence is primarily dictated by the characteristic time scale for star formation. In the more contemporary hierarchical pictures of galaxy formation, these smooth histories would be punctuated by merger-induced starbursts, but the basic long-term histories would be similar, especially for the disks.

The *right panel* in Figure 8 shows the same star formation histories but transformed into SFRs as functions of redshift (assuming $\Omega = 0.3$ and a formation redshift $z_f = 5$). This diagram illustrates how the dominant star forming (massive) host galaxy populations might evolve with redshift. Most star formation at the present epoch resides in late-type gas-rich galaxies, but by $z \sim 1$, all spiral types are predicted to have comparable SFRs, and (present-day) early-type systems become increasingly dominant at higher redshifts. The tendency of early-type galaxies to have higher masses will make the change in population with redshift even stronger. It will be interesting to see whether these trends are observed in future look-back studies. Many readers are probably aware that the redshift dependence of the volume averaged SFR shows quite a different character, with a broad maximum between $z \sim 1-2$ and a decline at higher redshifts (Madau et al 1996, 1998). This difference probably reflects the importance of hierarchical processes such as mergers in the evolution of galaxies, mechanisms that are not included in the simple phenomenological description in Figure 8 (Pei & Fall 1995, Madau et al 1998).

5.2 Evolution of Circumnuclear Star Formation

The SFRs in the circumnuclear regions are largely decoupled from those of disks and show no strong relationship to either the gas contents or the bulge/disk properties of the parent galaxies. Instead, the nuclear SFRs are closely associated with dynamical influences such as gas transport by bars or external gravitational perturbations, which stimulate the flow of gas into the circumnuclear regions.

The temporal properties of the star formation in the nuclear regions show a wide variation. Approximately 80–90% of spiral nuclei in optically selected samples exhibit modest levels of Balmer emission, with an average H α emission-line equivalent width of 20–30 Å (Stauffer 1982, Kennicutt et al 1989b, Ho et al 1997a,b). This is comparable to the average value in the disks of late-type spiral galaxies and is in the range expected for constant star formation over the age of the disk (Kennicutt 1983a, Kennicutt et al 1994). Hence, most nuclei show SFRs consistent with steady-state or declining star formation, though it is likely that some of these nuclei are observed in a quiescent stage between major outbursts.

Starbursts are clearly the dominant mode of star formation in IR-selected samples of nuclei. The typical gas consumption times are in the range of 10^8-10^9 years (Figure 7), so the high SFRs can only be sustained for a small percentage of the Hubble time. These time scales can be extended if a steady supply is introduced from the outside, for example by a strong dissipative bar. The most luminous nuclear starbursts ($L_{bol} \geq 10^{12} L_{\odot}$) are singular events. Maintaining such luminosities for even 10^8 years requires a total gas mass on the order of $10^{10}-10^{11} M_{\odot}$, equivalent to the total gas supply in most galaxies.

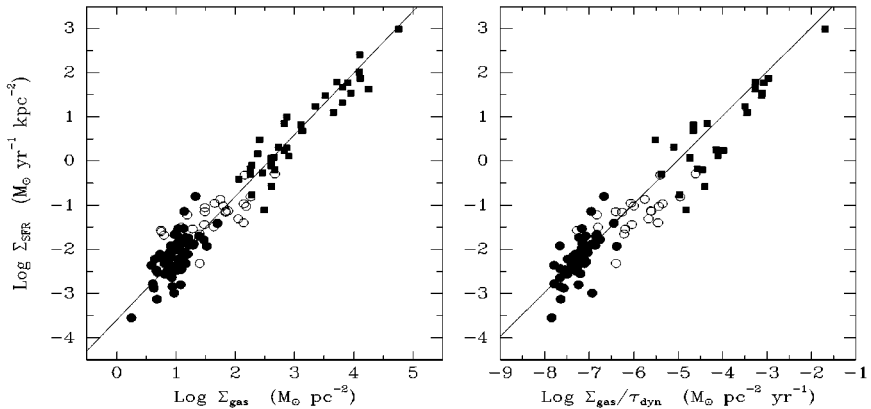


Figure 9 (Left) The global Schmidt law in galaxies. *Solid points* in Figure 5, *squares* denote the circumnuclear starbursts in Figure 7. The *open circles* show the SFRs and gas densities of the central regions of the normal disks. (Right) The same SFR data but plotted against the ratio of the gas density to the average orbital time in the disk. Both plots are adapted from Kennicutt (1998).

Violent interactions and mergers are the only events capable of triggering such a catastrophic mass transfer.

5.3 Physical Regulation of Star Formation Rate

Although star-forming galaxies span millionfold ranges in their present SFRs and physical conditions, there is a remarkable continuity in some of their properties, and these relationships provide important insights into the physical regulation of the SFR over this entire spectrum of activities.

We have already seen evidence from Figures 5 and 7 that the global SFRs of disks and nuclear starbursts are correlated with the local gas density, though over very different ranges in density and SFR per unit area. The *left panel* of Figure 9 shows both sets of data plotted on a common scale, and it reveals that the entire range of activities, spanning 5–6 orders of magnitude in gas and SFR densities, fits on a common power law with index $N \sim 1.4$ (Kennicutt 1998). The SFRs for the two sets of data were derived using separate methods ($\text{H}\alpha$ luminosities for the normal disks and FIR luminosities for the starbursts), and to verify that they are measured on a self-consistent scale, Figure 9 also shows $\text{H}\alpha$ -derived SFR gas densities for the centers (1–2 kpc) of the normal disks (plotted as *open circles*). The tight relation shows that a simple Schmidt (1959) power law provides an excellent empirical parametrization of the SFR, across an enormous range of SFRs, and it suggests that the gas density is the primary determinant of the SFR on these scales.

The uncertainty in the slope of the best-fitting Schmidt law is dominated by systematic errors in the SFRs, with the largest being the FIR-derived SFRs and CO-derived gas densities in the starburst galaxies. Changing either scale individually by a factor of two introduces a change of 0.1 in the fitted value of N , and this is a reasonable estimate of the systematic errors involved (Kennicutt 1998). Incorporating these uncertainties yields the following relation for the best-fitting Schmidt law:

$$\Sigma_{SFR} = (2.5 \pm 0.7) \times 10^{-4} \left(\frac{\Sigma_{gas}}{1 M_{\odot} \text{ pc}^{-2}} \right)^{1.4 \pm 0.15} M_{\odot} \text{ year}^{-1} \text{ kpc}^{-2}, \quad (7)$$

where Σ_{SFR} and Σ_{gas} are the disk-averaged SFR and gas surface densities, respectively.

As discussed by Larson (1992) and Elmegreen (1994), a large-scale Schmidt law with index $N \sim 1.5$ would be expected for self-gravitating disks if the SFR scales as the ratio of the gas density (ρ) to the free-fall time scale ($\propto \rho^{-0.5}$) and the average gas scale height is roughly constant across the sample ($\Sigma \propto \rho$). In a variant on this picture, Elmegreen (1997) and Silk (1997) have suggested that the SFR might scale with the ratio of the gas density to the average orbital time scale; this is equivalent to postulating that disks process a fixed fraction of their gas into stars in each orbit around the galactic center. The *right panel* of Figure 9, also adapted from Kennicutt (1998), shows the correlation between the SFR density and Σ_{gas}/τ_{dyn} for the same galaxies and starbursts. For this purpose τ_{dyn} is defined as one disk orbit time, measured at half of the outer radius of the star-forming disk, in units of years (see Kennicutt 1998 for details). The line is a median fit to the normal disks with slope constrained to unity, as predicted by the simple Silk model. This alternative “recipe” for the SFR provides a fit that is nearly as good as the Schmidt law. The equation of the fit is

$$\Sigma_{SFR} = 0.017 \Sigma_g \Omega_g. \quad (8)$$

In this parametrization, the SFR is simply $\sim 10\%$ of the available gas mass per orbit.

These parametrizations offer two distinct interpretations of the high SFRs in the centers of luminous starburst galaxies. In the context of the Schmidt law picture, the star formation efficiency scales as $\Sigma_g^{(N-1)}$, or $\Sigma_g^{0.4}$ for the observed relation in Figure 9. The central starbursts have densities that are on the order of 100–10,000 times higher than in the extended star-forming disks of spirals, so the global star formation efficiencies should be 6–40 times higher. Alternatively, in the kinematic picture, the higher efficiencies in the circumnuclear starbursts are simply a consequence of the shorter orbital time scales in the

galaxy centers, independent of the gas density. Whether the observed Schmidt law is a consequence of the shorter dynamical times or vice versa cannot be ascertained from these data alone, but either description provides an excellent empirical description or “recipe” for the observed SFRs.

These simple pictures can account for the high SFRs in the starburst galaxies, as well as for the observed radial variation of SFRs within star-forming disks (Kennicutt 1989, 1998). However the relatively shallow $N \sim 1.4$ Schmidt law cannot account for the strong changes in disk SFRs observed across the Hubble sequence if the disks evolved as nearly closed systems (Kennicutt et al 1994). Likewise, the modest changes in galaxy rotation curves with Hubble type are too small to account for the large differences in star formation histories with a kinematical model such as in Equation 8. The explanation probably involves star formation thresholds in the gas-poor galaxies (Kennicutt 1989, 1997), but the scenario has not been tested quantitatively, and it is possible that other mechanisms, such as infall of gas, merger history, or bulge-disk interactions are responsible for the strong changes in star formation histories across the spiral sequence.

6. FUTURE PROSPECTS

The observations described in this review have provided us with the beginnings of a quantitative picture of the star formation properties and evolutionary properties of the Hubble sequence. However, the picture remains primitive in many respects, as it is based in large part on integrated, one-zone averages over entire galaxies and extrapolations from present-day SFRs to crude characterizations of past star formation histories. Uncertainties in fundamental parameters such as the IMF and massive stellar evolution undermine the accuracy of the entire SFR scale and weaken the interpretations that are based on these measurements. Ongoing work on several fronts should lead to dramatic progress over the next decade, however.

The most exciting current development is the application of the SFR diagnostics described in Section 2 to galaxies spanning the full range of redshifts and look-back times (Ellis 1997). This work has already provided the first crude measures of the evolution in the volume-averaged SFR (Madau et al 1996, 1998). The combination of 8- to 10-m class groundbased telescopes, HST, and eventually the *Next Generation Space Telescope* should provide detailed inventories of integrated spectra, SFRs, and morphologies for complete samples of galaxies at successive redshifts. This should give the definitive picture of the star formation history of the Hubble sequence and impose strong tests on galaxy formation and evolution models. At the same time, a new generation of IR space observatories, including the *Wide-Field Infrared Explorer* and *Space Infrared Telescope Facility*, will provide high-resolution observations of nearby starburst

galaxies and the first definitive measurements of the cosmological evolution of the IR-luminous starburst galaxy population.

Although studies of the star formation histories of nearby galaxies are largely being supplanted by the more powerful look-back studies, observations of nearby galaxies will remain crucial for understanding many critical aspects of galaxy formation and evolution. Perhaps the greatest potential is for understanding the physical processes that determine the local and global SFRs in galaxies and understanding the feedback processes between the star formation and the parent galaxies. This requires spatially resolved measurements of SFRs over the full spectrum of interstellar and star formation environments and complementary measurements of the densities, dynamics, and abundances of the interstellar gas. Uncertainty about the nature of the star formation law and the SFR–ISM feedback cycle remain major stumbling blocks to realistic galaxy evolution models, but observations over the next decade should provide the foundations of a physically based model of galactic star formation and the Hubble sequence.

ACKNOWLEDGMENTS

I wish to express special thanks to my collaborators in the research presented here, especially my current and former graduate students Audra Baleisis, Fabio Bresolin, Charles Congdon, Murray Dixson, Kevin Edgar, Paul Harding, Crystal Martin, Sally Oey, Anne Turner, and Rene Walterbos. During the preparation of this review, my research was supported by the National Science Foundation through grant AST-9421145.

Visit the *Annual Reviews* home page at
<http://www.AnnualReviews.org>.

Literature Cited

- Aalto S, Booth RS, Black JH, Koribalski B, Wielebinski R. 1994. *Astron. Astrophys.* 286:365–80
- Athanassoula E. 1992. *MNRAS* 259:345–64
- Bagnuolo WG. 1976. *The stellar content and evolution of irregular and other late-type galaxies*. PhD thesis. Calif. Inst. Technol., Pasadena
- Balzano VA. 1983. *Ap. J.* 268:602–27
- Barnes JE, Hernquist L. 1992. *Annu. Rev. Astron. Astrophys.* 30:705–42
- Bechtold J, Yee HKC, Elston R, Ellingson E. 1997. *Ap. J. Lett.* 477:L29–32
- Bertelli G, Bressan A, Chiosi C, Fagotto F, Nasi E. 1994. *Astron. Astrophys. Suppl.* 106:275–302
- Boselli A. 1994. *Astron. Astrophys.* 292:1–12
- Boselli A, Gavazzi G, Lequeux J, Buat V, Casoli F, et al. 1995. *Astron. Astrophys.* 300:L13–16
- Bothun GD. 1990. In *Evolution of the Universe of Galaxies*, ed. RG Kron, *ASP Conf. Proc.* 10:54–66. San Francisco: Astron. Soc. Pac.
- Bresolin F, Kennicutt RC. 1997. *Astron. J.* 113:975–80
- Bruzual G, Charlot S. 1993. *Ap. J.* 405:538–53
- Buat V. 1992. *Astron. Astrophys.* 264:444–54
- Buat V, Deharveng JM. 1988. *Astron. Astrophys.* 195:60–70
- Buat V, Deharveng JM, Donas J. 1989. *Astron. Astrophys.* 223:42–46

- Buat V, Xu C. 1996. *Astron. Astrophys.* 306:61–72
- Bushouse HA. 1986. *Astron. J.* 91:255–70
- Bushouse HA. 1987. *Ap. J.* 320:49–72
- Bushouse HA, Werner MW, Lamb SA. 1988. *Ap. J.* 335:74–92
- Caldwell N, Kennicutt R, Phillips AC, Schommer RA. 1991. *Ap. J.* 370:526–40
- Caldwell N, Kennicutt R, Schommer R. 1994. *Astron. J.* 108:1186–90
- Calzetti D. 1997. *Astron. J.* 113:162–84
- Calzetti D, Kinney AL, Storchi-Bergmann T. 1994. *Ap. J.* 429:582–601
- Calzetti D, Kinney AL, Storchi-Bergmann T. 1996. *Ap. J.* 458:132–35
- Caplan J, Deharveng L. 1986. *Astron. Astrophys.* 155:297–313
- Caplan J, Ye T, Deharveng L, Turtle AJ, Kennicutt RC. 1996. *Astron. Astrophys.* 307:403–16
- Carico DP, Sanders DB, Soifer BT, Matthews K, Neugebauer G. 1990. *Astron. J.* 100:70–83
- Cayatte V, Kotanyi C, Balkowski C, van Gorkom JH. 1994. *Astron. J.* 107:1003–17
- Cepa J, Beckman JE. 1990. *Ap. J.* 349:497–502
- Charlot S, Bruzual G. 1991. *Ap. J.* 367:126–40
- Cohen JG. 1976. *Ap. J.* 203:587–92
- Cox P, Mezger PG. 1989. *Astron. Astrophys. Rev.* 1:49–83
- Cowie LL, Hu EM, Songaila A, Egami E. 1997. *Ap. J. Lett.* 481:L9–13
- Cowie LL, Songaila A, Hu EM, Cohen JG. 1996. *Astron. J.* 112:839–64
- Cutri RM, McAlary CW. 1985. *Ap. J.* 296:90–105
- Deharveng JM, Sasseen TP, Buat V, Bowyer S, Lampton M, Wu X. 1994. *Astron. Astrophys.* 289:715–28
- de Vaucouleurs G, de Vaucouleurs A, Corwin HG. 1976. *Second Reference Catalog of Bright Galaxies*. Austin: Univ. Tex. Press
- Devereux N. 1987. *Ap. J.* 323:91–107
- Devereux NA, Becklin EE, Scoville N. 1987. *Ap. J.* 312:529–41
- Devereux NA, Hameed S. 1997. *Astron. J.* 113:599–608
- Devereux NA, Young JS. 1990. *Ap. J. Lett.* 350:L25–L28
- Devereux NA, Young JS. 1991. *Ap. J.* 371:515–24
- Donas J, Deharveng JM. 1984. *Astron. Astrophys.* 140:325–33
- Donas J, Deharveng JM, Laget M, Milliard B, Huguenin D. 1987. *Astron. Astrophys.* 180:12–26
- Donas J, Milliard B, Laget M. 1995. *Astron. Astrophys.* 303:661–672
- Donas J, Milliard B, Laget M, Buat V. 1990. *Astron. Astrophys.* 235:60–68
- Downes D, Solomon PM, Radford SJE. 1993. *Ap. J. Lett.* 414:L13–L16
- Dressel LL. 1988. *Ap. J. Rev.* 329:L69–L73
- Dressler A. 1984. *Annu. Rev. Astron. Astrophys.* 22:185–222
- Ellis RS. 1997. *Annu. Rev. Astron. Astrophys.* 35:389–443
- Elmegreen BG. 1994. *Ap. J. Lett.* 425:L73–L76
- Elmegreen BG. 1997. In *Starburst Activity in Galaxies*, ed. J Franco, R Terlevich, A Serrano, *Rev. Mex. Astron. Astrophys. Conf. Ser.* 6:165–71
- Elmegreen BG, Elmegreen DM. 1986. *Ap. J.* 311:554–62
- Engelbracht CW. 1997. *Infrared observations and stellar populations modelling of starburst galaxies*. PhD thesis, Univ. Arizona, Tempe
- Evans IN, Koratkar AP, Storchi-Bergmann T, Kirkpatrick H, Heckman TM, Wilson AS. 1996. *Ap. J. Suppl.* 105:93–127
- Fanelli MN, Marcum PM, Waller WH, Cornett RH, O’Connell RW, et al. 1998. In *The Ultraviolet Universe at Low and High Redshift*, ed. W Waller, M Fanelli, J Hollis, A Danks, *AIP Conf.* 408. New York: Am. Inst. Phys. In press
- Feinstein C. 1997. *Ap. J. Suppl.* 112:29–47
- Ferguson AMN, Wyse RFG, Gallagher JS, Hunter DA. 1996. *Astron. J.* 111:2265–79
- Fioc M, Rocca-Volmerange B. 1997. *Astron. Astrophys.* 326:950–62
- Friedli D, Benz W. 1995. *Astron. Astrophys.* 301:649–65
- Gallagher JS, Hunter DA. 1984. *Annu. Rev. Astron. Astrophys.* 22:37–74
- Gallagher JS, Hunter DA, Bushouse H. 1989. *Astron. J.* 97:700–7
- Gallagher JS, Hunter DA, Tutukov AV. 1984. *Ap. J.* 284:544–56
- Gallego J, Zamorano J, Aragon-Salamanca A, Rego M. 1995. *Ap. J. Lett.* 445:L1–L4
- Gallimore JF, Keel WC. 1993. *Astron. J.* 106:1337–43
- Gavazzi G, Boselli A, Kennicutt R. 1991. *Astron. J.* 101:1207–30
- Gavazzi G, Jaffe W. 1985. *Ap. J. Lett.* 294:L89–L92
- Gavazzi G, Pierini D, Boselli A. 1996. *Astron. Astrophys.* 312:397–408
- Gavazzi G, Scodreggio M. 1996. *Astron. Astrophys.* 312:L29–L32
- Gilmore GF, Parry IR, Howell DJ, eds. 1998. *The Stellar Initial Mass Function*. San Francisco: Astron. Soc. Pac. In press
- Giuricin G, Tamburini L, Mardirossian F, Mezzetti M, Monaco P. 1994. *Astron. Astrophys.* 427:202–20
- Goldader JD, Joseph RD, Doyon R, Sanders DB. 1995. *Ap. J.* 444:97–112

- Goldader JD, Joseph RD, Doyon R, Sanders DB. 1997. *Ap. J. Suppl.* 108:449–70
- González Delgado RM, Perez E, Tadhunter C, Vilchez J, Rodríguez-Espinoza JM. 1997. *Ap. J. Suppl.* 108:155–98
- Harper DA, Low FJ. 1973. *Ap. J. Lett.* 182:L89–L93
- Hawarden TG, Mountain CM, Leggett SK, Puxley PJ. 1986. *MNRAS* 221:41–45P
- Haynes MP, Giovanelli R, Chincarini GL. 1984. *Annu. Rev. Astron. Astrophys.* 22:445–70
- Heckman TM. 1990. In *Paired and Interacting Galaxies, IAU Colloq. 124*, ed. JW Sulentic, WC Keel, CM Telesco, NASA Conf. Publ. CP-3098, pp. 359–82. Washington, DC: Natl. Aeronaut. Space Admin.
- Heckman TM. 1994. In *Mass-Transfer Induced Activity in Galaxies*, ed. I Shlosman, pp. 234–50. Cambridge, UK: Cambridge Univ. Press
- Heckman TM, Crane PC, Balick B. 1980. *Astron. Astrophys. Suppl.* 40:295–305
- Heiles C. 1990. *Ap. J.* 354:483–91
- Ho LC, Filippenko AV, Sargent WLW. 1997a. *Ap. J.* 487:579–90
- Ho LC, Filippenko AV, Sargent WLW. 1997b. *Ap. J.* 487:591–602
- Ho PTP, Beck SC, Turner JL. 1990. *Ap. J.* 349:57–66
- Hodge PW. 1989. *Annu. Rev. Astron. Astrophys.* 27:139–59
- Hodge PW, Kennicutt RC. 1983. *Astron. J.* 88:296–328
- Huang JH, Gu QS, Su HJ, Hawarden TG, Liao XH, Wu GX. 1996. *Astron. Astrophys.* 313:13–24
- Hubble E. 1926. *Ap. J.* 64:321–69
- Huchra JP. 1977. *Ap. J.* 217:928–39
- Hunter DA. 1994. *Astron. J.* 107:565–81
- Hunter DA, Gallagher JS. 1985. *Ap. J. Suppl.* 58:533–60
- Hunter DA, Gallagher JS. 1990. *Ap. J.* 362:480–90
- Hunter DA, Gillett FC, Gallagher JS, Rice WL, Low FJ. 1986. *Ap. J.* 303:171–85
- Hunter DA, Hawley WN, Gallagher JS. 1993. *Astron. J.* 106:1797–811
- Isobe T, Feigelson E. 1992. *Ap. J. Suppl.* 79:197–211
- Israel FP, van der Hulst JM. 1983. *Astron. J.* 88:1736–48
- Joseph RD, Wright GS. 1985. *MNRAS* 214:87–95
- Kaufman M, Bash FN, Kennicutt RC, Hodge PW. 1987. *Ap. J.* 319:61–75
- Keel WC. 1983. *Ap. J.* 269:466–86
- Keel WC, Kennicutt RC, Hummel E, van der Hulst JM. 1985. *Astron. J.* 90:708–30
- Kennicutt RC. 1983a. *Ap. J.* 272:54–67
- Kennicutt RC. 1983b. *Astron. J.* 88:483–88
- Kennicutt RC. 1989. *Ap. J.* 344:685–703
- Kennicutt RC. 1992a. *Ap. J.* 388:310–27
- Kennicutt RC. 1992b. *Ap. J. Suppl.* 79:255–84
- Kennicutt RC. 1997. In *The Interstellar Medium in Galaxies*, ed. JM van der Hulst, pp. 171–95. Dordrecht: Kluwer
- Kennicutt RC. 1998. *Ap. J.* In press
- Kennicutt RC, Bothun GD, Schommer RA. 1984. *Astron. J.* 89:1279–87
- Kennicutt RC, Bresolin F, Bomans DJ, Bothun GD, Thompson IB. 1995. *Astron. J.* 109:594–604
- Kennicutt RC, Edgar BK, Hodge PW. 1989a. *Ap. J.* 337:761–81
- Kennicutt RC, Keel WC, Blaha CA. 1989b. *Astron. J.* 97:1022–35
- Kennicutt RC, Keel WC, van der Hulst JM, Hummel E, Roettiger KA. 1987. *Astron. J.* 93:1011–23
- Kennicutt RC, Kent SM. 1983. *Astron. J.* 88:1094–107
- Kennicutt RC, Tamblyn P, Congdon CW. 1994. *Ap. J.* 435:22–36
- Kennicutt RC, Schweizer F, Barnes JE. 1998. In *Galaxies: Interactions and Induced Star Formation, Saas-Fee Advanced Course 26*, ed. D Friedli, L Martinet, D Pfenniger. Berlin: Springer. In press
- Kinney AL, Bohlin RC, Calzetti D, Panagia N, Wyse RFG. 1993. *Ap. J. Suppl.* 86:5–93
- Klein U, Grave R. 1986. *Astron. Astrophys.* 161:155–68
- Knapen J, Beckman JE, Cepa J, van der Hulst JM, Rand RJ. 1992. *Ap. J. Lett.* 385:L37–L40
- Larson RB. 1992. In *Star Formation in Stellar Systems*, ed. G Tenorio-Tagle, M Prieto, F Sánchez, pp. 125–90. Cambridge, UK: Cambridge Univ. Press
- Larson RB, Tinsley BM. 1978. *Ap. J.* 219:46–59
- Lawrence A, Rowan-Robinson M, Leech K, Jones DHP, Wall JV. 1989. *MNRAS* 240:329–48
- Leech M, Rowan-Robinson M, Lawrence A, Hughes JD. 1994. *MNRAS* 267:253–69
- Lehnert MD, Heckman TM. 1996. *Ap. J.* 472:546–63
- Leitherer C, Alloin D, Alvensleben UF, Gallagher JS, Huchra JP, et al. 1996a. *Publ. Astron. Soc. Pac.* 108:996–1017
- Leitherer C, Ferguson HC, Heckman TM, Lowenthal JD. 1995a. *Ap. J. Lett.* 454:L19–L22
- Leitherer C, Fritze-v. Alvensleben U, Huchra JP, eds. 1996b. *From Stars to Galaxies: The Impact of Stellar Physics on Galaxy Evolution*, Vol. 98. San Francisco: Astron. Soc Pac.
- Leitherer C, Heckman TM. 1995. *Ap. J. Suppl.* 96:9–38
- Leitherer C, Robert C, Heckman TM. 1995b. *Ap. J. Suppl.* 99:173–87
- Liu CT, Kennicutt RC. 1995. *Ap. J.* 450:547–58
- Lonsdale CJ, Helou G. 1987. *Ap. J.* 314:513–24

- Lonsdale CJ, Persson SE, Matthews K. 1984. *Ap. J.* 287:95–107
- Lutz D, Genzel R, Sternberg A, Netzer H, Kunze D, et al. 1996. *Astron. Astrophys.* 315:L137–40
- Madau P, Ferguson H, Dickinson M, Giavalisco M, Steidel CC, Fruchter A. 1996. *MNRAS* 283:1388–404
- Madau P, Pozzetti L, Dickinson M. 1998. *Ap. J.* In press
- Maoz D, Filippenko AV, Ho LC, Macchetto D, Rix H-W, Schneider DP. 1996. *Ap. J. Suppl.* 107:215–26
- Martin CL. 1998. *Ap. J.* In press
- Martinet L, Friedli D. 1997. *Astron. Astrophys.* 323:363–73
- Massey P. 1998. In *The Stellar Initial Mass Function*, ed. BF Gilmore, IR Parry, DJ Howell. San Francisco: Astron. Soc. Pac. In press
- McCall ML, Schmidt FH. 1986. *Ap. J.* 311:548–53
- Meurer GR, Gerhardt R, Heckman TM, Lehnert MD, Leitherer C, Lowenthal J. 1997. *Astron. J.* 114:54–68
- Meurer GR, Heckman TM, Leitherer C, Kinney A, Robert C, Garnett DR. 1995. *Astron. J.* 110:2665–91
- Mihos JC, Hernquist L. 1996. *Ap. J.* 464:641–63
- Morgan WW. 1958. *Publ. Astron. Soc. Pac.* 70:364–91
- Moshir M, Kopan G, Conrow J, McCallon H, Hacking P, et al. 1992. *Explanatory Supplement to the IRAS Faint Source Survey, Version 2*, JPL D-10015 8/92. Jet Prop. Lab., Pasadena, Calif.
- Moss C, Whittle M. 1993. *Ap. J. Lett.* 200 407:L17–L20
- Niklas S, Klein U, Braine J, Wielebinski R. 1995. *Astron. Astrophys. Suppl.* 114:21–49
- Niklas S, Klein U, Wielebinski R. 1997. *Astron. Astrophys.* 322:19–28
- Norman CA, Ikeuchi S. 1989. *Ap. J.* 345:372–83
- Oey MS, Kennicutt RC. 1997. *MNRAS*. In press
- Ostriker JP, Thuan TX. 1975. *Ap. J.* 202:353–64
- Patel K, Wilson CD. 1995a. *Ap. J.* 451:607–15
- Patel K, Wilson CD. 1995b. *Ap. J.* 453:162–72
- Pei YC, Fall SM. 1995. *Ap. J.* 454:69–76
- Phillips AC. 1993. *Star formation in barred spiral galaxies*. PhD thesis. Univ. Washington, Seattle
- Pogge RW, Eskridge PB. 1987. *Astron. J.* 93: 291–300
- Pogge RW, Eskridge PB. 1993. *Astron. J.* 106: 1405–19
- Pompea SM, Rieke GH. 1990. *Ap. J.* 356:416–29
- Puxley PJ, Brand PWJL, Moore TJT, Mountain CM, Nakai N, Yamashita AT. 1989. *Ap. J.* 345:163–68
- Puxley PJ, Hawarden TG, Mountain CM. 1990. *Ap. J.* 364:77–86
- Rieke GH, Lebofsky MJ. 1978. *Ap. J. Lett.* 220:L37–L41
- Rieke GH, Lebofsky MJ. 1979. *Annu. Rev. Astron. Astrophys.* 17:477–511
- Rieke GH, Loken K, Rieke MJ, Tamblyn P. 1993. *Ap. J.* 412:99–110
- Rieke GH, Low FJ. 1972. *Ap. J. Lett.* 176:L95–L100
- Roberts MS. 1963. *Annu. Rev. Astron. Astrophys.* 1:149–78
- Roberts MS, Haynes MP. 1994. *Annu. Rev. Astron. Astrophys.* 32:115–52
- Romanishin W. 1990. *Astron. J.* 100:373–76
- Rowan-Robinson M, Crawford J. 1989. *MNRAS* 238:523–58
- Rubin VC, Kenney JDP, Young JS. 1997. *Astron. J.* 113:1250–78
- Ryder SD. 1993. *Massive star formation in galactic disks*. PhD thesis. Aust. Natl. Univ., Canberra
- Ryder SD, Dopita MA. 1993. *Ap. J. Suppl.* 88:415–21
- Ryder SD, Dopita MA. 1994. *Ap. J.* 430:142–62
- Salpeter EE. 1955. *Ap. J.* 121:161–67
- Sandage A. 1986. *Astron. Astrophys.* 161:89–101
- Sanders DB, Mirabel IF. 1996. *Annu. Rev. Astron. Astrophys.* 34:749–92
- Sanders DB, Scoville NZ, Soifer BT. 1991. *Ap. J.* 370:158–71
- Sanders DB, Soifer BT, Elias JH, Madore BF, Matthews K, et al. 1988. *Ap. J.* 325:74–91
- Sauvage M, Thuan TX. 1992. *Ap. J. Lett.* 396: L69–L73
- Sauvage M, Thuan TX. 1994. *Ap. J.* 429:153–71
- Scalo JM. 1986. *Fundam. Cosm. Phys.* 11:1–278
- Schmidt M. 1959. *Ap. J.* 129:243–58
- Scoville NZ, Becklin EE, Young JS, Capps RW. 1983. *Ap. J.* 271:512–23
- Scoville NZ, Hibbard JE, Yun MS, van Gorkom JH. 1994. In *Mass-Transfer Induced Activity in Galaxies*, ed. I Shlosman, pp.191–212. Cambridge, UK: Cambridge Univ. Press
- Searle L, Sargent WLW, Bagnuolo WG. 1973. *Ap. J.* 179:427–38
- Sérsic JL, Pastoriza M. 1967. *Publ. Astron. Soc. Pac.* 79:152–55
- Silk J. 1997. *Ap. J.* 481:703–9
- Smith AM, Cornett RH. 1982. *Ap. J.* 261:1–11
- Smith BJ, Harvey PM. 1996. *Ap. J.* 468:139–66
- Smith EP, Pica AJ, Bohlin RC, Cornett RH, Fanelli MN. 1996. *Ap. J. Suppl.* 104:207–315
- Soifer BT, Houck JR, Neugebauer G. 1987. *Annu. Rev. Astron. Astrophys.* 25:187–230
- Solomon PM, Downes D, Radford SJE, Barrett JW. 1997. *Ap. J.* 478:144–61

- Solomon PM, Sage LJ. 1988. *Ap. J.* 334:613–25
- Stauffer JR. 1982. *Ap. J. Suppl.* 50:517–27
- Steidel CC, Giavalisco M, Pettini M, Dickinson M, Adelberger KL. 1996. *Ap. J. Lett.* 462:L17–L21
- Telesco CM. 1988. *Annu. Rev. Astron. Astrophys.* 26:343–76
- Telesco CM, Dressel LL, Wolstencroft RD. 1993. *Ap. J.* 414:120–43
- Telesco CM, Harper DA. 1980. *Ap. J.* 235:392–404
- Telesco CM, Wolstencroft RD, Done C. 1988. *Ap. J.* 329:174–86
- Thronson HA, Bally J, Hacking P. 1989. *Astron. J.* 97:363–74
- Tinney CG, Scoville NZ, Sanders DB, Soifer BT. 1990. *Ap. J.* 362:473–79
- Tinsley BM. 1968. *Ap. J.* 151:547–65
- Tinsley BM. 1972. *Astron. Astrophys.* 20:383–96
- Tomita A, Tomita Y, Saito M. 1996. *Pub. Astron. Soc. J.* 48:285–303
- Tully RB, Mould JR, Aaronson M. 1982. *Ap. J.* 257:527–37
- Turner JL, Ho PTP. 1994. *Ap. J.* 421:122–39
- van der Hulst JM, Kennicutt RC, Crane PC, Rots AH. 1988. *Astron. Astrophys.* 195:38–52
- Veilleux S, Kim D-C, Sanders DB, Mazzarella JM, Soifer BT. 1995. *Ap. J. Suppl.* 98:171–217
- Waller W, Fanelli M, Danks A, Hollis J, eds. 1997. *The Ultraviolet Universe at Low and High Redshift, AIP Conf.* 408. New York: Am. Inst. Phys. In press
- Walterbos RAM, Braun R. 1994. *Ap. J.* 431:156–71
- Walterbos RAM, Greenawalt B. 1996. *Ap. J.* 460:696–710
- Warmels RH. 1988. *Astron. Astrophys. Suppl.* 72:427–47
- Weedman DW, Feldman FR, Balzano VA, Ramsey LW, Sramek RA, Wu C-C. 1981. *Ap. J.* 248:105–12
- Whitford AE. 1975. In *Galaxies in the Universe*, ed. A Sandage, M Sandage, J Kristian, *Stars Stellar Syst. Compend.*, 9:159–76. Chicago: Univ. Chicago Press
- Wright GS, Joseph RD, Robertson NA, James PA, Meikle WPS. 1988. *MNRAS* 233:1–23
- Wyse RFG. 1983. *MNRAS* 199:1P–8P
- Xu C, Sulentic JW. 1991. *Ap. J.* 374:407–30
- Young JS, Allen L, Kenney JDP, Lesser A, Rownd B. 1996. *Astron. J.* 112:1903–27
- Young JS, Schloerb FP, Kenney JDP, Lord SD. 1986. *Ap. J.* 304:443–58
- Young JS, Scoville NZ. 1991. *Annu. Rev. Astron. Astrophys.* 29:581–625